

# CdS Quantum Dots as Potent Photoreductants for Organic Chemistry Enabled by Auger Recombination

*Jonas K. Widness,<sup>†</sup> Daniel G. Enny,<sup>†</sup> Kaelyn S. McFarlane-Connelly,<sup>‡</sup> Mahilet T. Miedenbauer,<sup>§</sup> Todd D. Krauss,<sup>‡§^</sup> and Daniel J. Weix<sup>\*†</sup>*

<sup>†</sup>Department of Chemistry, UW-Madison, Madison, WI 53706 USA

<sup>‡</sup>Department of Chemistry, University of Rochester, Rochester, NY 14627 USA

<sup>§</sup>Materials Science Program, University of Rochester, Rochester, NY 14627 USA

<sup>^</sup>Institute of Optics, University of Rochester, Rochester, NY 14627 USA

**ABSTRACT:** Strong reducing agents ( $< -2.0$  V vs SCE) enable a wide array of useful organic chemistry, but suffer from a variety of limitations. Stoichiometric metallic reductants such as alkali metals and  $\text{SmI}_2$  are commonly employed for these reactions, however considerations including expense, ease of use, safety, and waste generation limit the practicality of these methods. Recent approaches utilizing energy from multiple photons or electron-primed photoredox catalysis have accessed reduction potentials equivalent to  $\text{Li}^0$  and shown how this enables selective transformations of aryl chlorides via aryl radicals. However, in some cases low stability of catalytic intermediates can limit turnover numbers. Herein we report the ability of

CdS nanocrystal quantum dots (QDs) to function as strong photoreductants and present evidence that a highly reducing electron is generated from two consecutive photoexcitations of CdS QDs with intermediate reductive quenching. Mechanistic experiments suggest that Auger recombination, a photophysical phenomenon known to occur in photoexcited anionic QDs, generates transient thermally excited electrons to enable the observed reductions. Using blue LEDs and sacrificial amine reductants, aryl chlorides and phosphate esters with reduction potentials up to -3.4 V vs. SCE are photo-reductively cleaved to afford hydrodefunctionalized or functionalized products. In contrast to small molecule catalysts, the QDs are stable under these conditions and turnover numbers up to 47500 have been achieved. These conditions can also effect other challenging reductions, such as tosylate protecting group removal from amines, debenzylolation of alcohols, and reductive ring-opening of cyclopropanecarboxylic acid derivatives.

## **Introduction**

Photoredox catalysis has changed the way chemists think about the reactivity of common functional groups by allowing photon-gated redox events or energy transfer to catalytically convert stable substrate functionalities into reactive intermediates.<sup>1,2</sup> Over time, structural elaboration of organic and organometallic dyes has produced a collection of effective photoredox catalysts with diverse photochemical characteristics.<sup>3,4</sup> By expanding the electrochemical horizons of photocatalysts, increasingly inert classes of chemicals have become accessible substrates for photoredox transformations. However, the maximum energy of a visible photon (3.1 eV at 400 nm), energy losses through catalyst intersystem crossing, and other nonradiative pathways impose limits on the strength of photogenerated redox agents from single visible photon absorption (Figure 1A).<sup>5-7</sup> Higher-energy UV irradiation can be used to generate

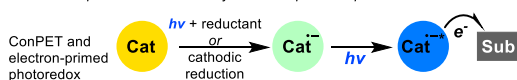
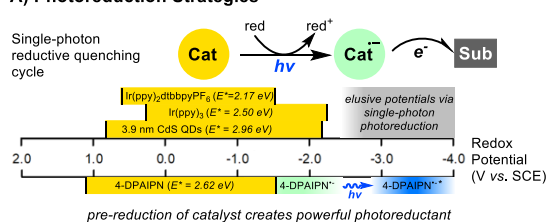
powerful redox agents,<sup>8,9</sup> however undesired photochemical side reactions limit the functional group tolerance of these approaches.<sup>10</sup>

To overcome these limitations, recent innovations have provided catalytic methods allowing the input of additional energy beyond a single visible photon to generate extremely strong reducing agents (Figure 1A). Beginning with seminal reports by König in 2014, many investigators have uncovered photocatalysts capable of consecutive photoinduced electron-transfer (conPET) events to harness the energy from multiple photons within a single catalyst turnover, wherein initial photoexcitation and reductive quenching of the photocatalyst produces a reduced catalyst species that can absorb a second photon to form a powerfully reducing excited state.<sup>1,6,11–13</sup> While this strategy has unlocked new photocatalyzed reductive transformations, conPET procedures present their own challenges. The photocatalyst must absorb visible photons of similar wavelengths in the ground state and after conversion to the active photoreductant via reduction, while additionally having appropriate excited state properties to drive chemistry after each successive excitation.<sup>6,13</sup> In complement to this advance, Lambert, Lin, Wickens, and others have pioneered electrochemical reduction of suitable precatalysts to form highly potent “electrochemically primed” photoredox catalysts.<sup>14–18</sup> By decoupling catalyst reduction from photoexcitation, this approach has greatly expanded the pool of competent reduction-activated photoreductants to include more accessible catalysts<sup>19</sup> and enabled new selective aryl radical chemistry by spatially separating the reaction mixture from potentially problematic reductants.

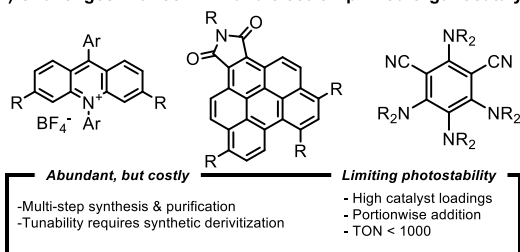
Still, challenges remain for each of these approaches (Figure 1B). High catalyst loadings are currently required for most conPET and electron-primed photoredox procedures (5–10 mol% is typical),<sup>20</sup> owing to the tendency for the reduced catalyst intermediates to decompose.<sup>19,21,22</sup> Electrochemistry-primed photoredox catalysis requires a more complex apparatus, leading to

challenges in vessel design and scalability. Moreover, the optimal organocatalysts for some strategies require multi-step syntheses and purification,<sup>13,23,24</sup> and can be expensive to use in significant quantities. Therefore, while these strategies have enabled redox-initiated transformations of substrates far beyond the potentials accessible by traditional photocatalysis, these early reports underscore the need for improved photocatalysts with additional stability and access to new mechanisms of reactivity.

#### A) Photoreduction Strategies



#### B) Challenges with conPET and electron-primed organocatalysts



#### C) This Work: CdS QDs as robust conPET photoreductants through Auger recombination

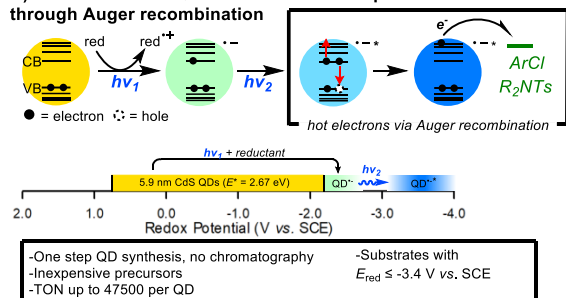


**Figure 1.** A: Contemporary strategies for photoredox-mediated reductions B: Commonly encountered challenges to existing photoreduction protocols C: This work: CdS QDs as robust highly-reducing ConPET photocatalysts for reductive organic transformations enabled by Auger recombination

Semiconductor quantum dots (QDs) combine advantageous aspects of both homogeneous (high surface-volume ratio, solubility in reaction media, light penetration) and heterogeneous (durability, substrate binding) catalysts, and therefore offer new opportunities for photoredox catalysis.<sup>25,26</sup> QDs have proven to be robust fluorophores and photocatalysts, generally exhibiting superior photostability to small-molecule dyes,<sup>27–33</sup> however applications of QDs to organic synthesis remain underexplored. To address the need for continued development of photoredox catalysts, our group and others have been interested in new applications of QDs in organic chemistry.<sup>26,34–61</sup> In addition to their high photostability, QDs exhibit tunable, size-dependent optical and redox properties; are made in single-step syntheses with no chromatography from abundant precursors;<sup>62</sup> reversibly bind to many molecules at once (typically 1 – 5 ligands/nm<sup>2</sup> of QD surface are found for closely related CdSe QDs<sup>63–65</sup>) through common organic functional groups (-CO<sub>2</sub>H, -PO<sub>3</sub>H, -SH, -NH<sub>2</sub>); can become charged with many electrons at once without decomposing;<sup>66,67</sup> and undergo many electronic processes with no direct analogue in small-molecules.<sup>68</sup>

Inspired by reports of conPET-type photoreduction mechanisms operative within commonly used photocatalyst systems,<sup>12,24,69</sup> we envisioned that QDs could achieve a similar mode of reactivity, while also addressing the catalyst stability and availability challenges of organocatalyst-mediated photoreductions. In particular, we considered that Auger recombination processes, a family of electronic events inaccessible to small-molecule photocatalysts which generate excited charge carriers from carrier recombination of trion or biexciton states,<sup>70–73</sup> could be used to drive energetically demanding photoreductions of organic molecules (Figure 1C). Photoexcitation of a QD followed by reductive quenching from a suitable terminal reductant produces a “photodoped” QD.<sup>74</sup> This is an anionic QD with the surplus electron residing in the

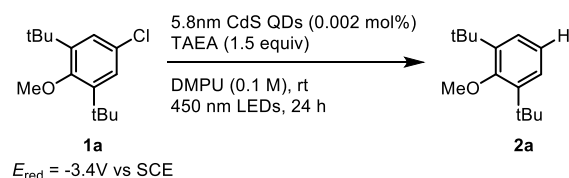
1S<sub>e</sub> state at the conduction band (CB) edge. The negatively charged QD can absorb a second photon at the same wavelength to produce an excited anionic “negative trion” state, with two electrons in the 1S<sub>e</sub> state and an electron-vacancy (“hole”) at the valence band (VB) edge. Negative trion states rapidly undergo Auger recombination (typically  $\tau < 100$  ps)<sup>71,75,76</sup> on timescales that are significantly faster than photoluminescence lifetimes. In Auger recombination, one 1S<sub>e</sub> electron acquires a kinetic energy equivalent to that of the exciton at the band gap, concomitant with relaxation of the other CB electron to the valence band edge, generating a highly energetic or “hot” electron (Figure 1C). While short lived,<sup>68,77</sup> these highly reducing “hot” electrons can be transferred to nearby or adsorbed species, and have been employed to improve aqueous hydrogen evolution and CO<sub>2</sub> reduction.<sup>73,78–80</sup> Auger processes are well studied phenomena in nanomaterials, however they have not been employed to drive synthetic organic transformations requiring powerful reducing agents. We show here that CdS QDs can be employed as powerful photoreductants for organic synthesis through a two-photon mechanism involving Auger recombination to generate hot electrons.

## Results

Initial studies revealed that oleate capped 5.8 - 6.0 nm CdS QDs<sup>81</sup> were capable photocatalysts for reductive dehalogenation of electron-neutral and -rich aryl chlorides with reduction potentials up to 1300 mV more negative than the most-negative reported reduction potential of CdS QDs ( $E_{\text{pc}}^{\text{QD/QD}^-} = -2.24$  V vs SCE for 4.0 nm CdS QDs).<sup>82,83</sup> To interrogate the photoreductive power of CdS QDs, optimization studies were undertaken using the reductive hydrodechlorination of 4-chloro-2,6-di-*tert*-butylanisole (**1a**) ( $E_{\text{red}} = -3.4$  V vs. SCE) as a challenging model reaction.<sup>14</sup> Optimization of the reaction conditions revealed that polar aprotic solvents performed best and *N,N'*-dimethylpropylene urea (DMPU) provided the highest yields of dehalogenated product.

Among the reductants examined, tris(2-aminoethyl)amine (TAEA), sodium formate, and *N,N*-diisopropylethylamine (DIPEA) were all effective, although TAEA was the most general (Table 1, entries 1-5). Lowering the QD loading slowed the reaction rate (entry 6), while control experiments showed that QDs, reductant, and light are all required for dehalogenation activity (entries 7-9). Despite their ability to coordinate to QD surfaces, the reductants NaSPh<sup>52</sup> and ethylenediaminetetraacetic acid<sup>84</sup> were ineffective under these reaction conditions. For additional optimization data, see the Supporting Information (Figure S1).

**Table 1. Optimization of Hydrodechlorination Reaction**



Entry	Conditions	Yield of <b>2a</b> <sup>a</sup>
1	As above	95%
2	4 equiv TAEA	68%
3	0.25 M	86%
4	4 equiv DIPEA instead of TAEA	91%
5	3 equiv NaCHO <sub>2</sub> instead of TAEA	95%
6	0.001 mol% QDs	74%
7	No light	0%
8	No QDs	0%
9	No reductant	0%
10	Ir(ppy) <sub>3</sub> (1 mol%) instead of QDs	2%
11	Bulk CdS (10 mol%) instead of QDs	0%

<sup>a</sup> Corrected GC yields using 0.1 mmol of **1a**. LED setups delivered 520 mW of 450 nm light to the reaction vessel. <sup>b</sup> Reaction conducted with 4 mmol **1a** in Penn PhD M2 photoreactor for 96 h. See SI for details.

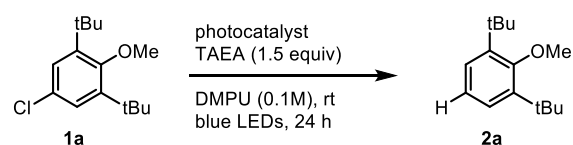
Substituting CdS QDs for Ir(ppy)<sub>3</sub>, among the most-reducing of commonly used molecular photocatalysts, resulted in only trace product formation (entry 10), despite exhibiting a similar reduction potential to CdS QDs ( $E_{1/2}^{III/II} = -2.19$  V vs SCE for Ir(ppy)<sub>3</sub>;  $E_{pc}^{QD/QD^-} = -2.15$  V vs SCE for 3.9 nm CdS QDs)<sup>82</sup> and a much longer excited state lifetime ( $\tau = 1.3$   $\mu$ s for Ir(ppy)<sub>3</sub> vs.  $\sim 10$  ns for Cd chalcogenide QDs).<sup>85–87</sup> While bulk semiconductors have seen increasing utility in photoredox catalysis,<sup>88–90</sup> in this case CdS QDs outperformed an equal mass of bulk CdS powder (entry 11), showing that the catalyst morphology and quantum properties play a role in dehalogenation activity. Auger processes are vanishingly inefficient in bulk semiconductors,<sup>91,92</sup> consistent with the inactivity of bulk CdS powder for photoreduction beyond its reduction potential. The reaction could be performed on gram-scale, although this required high intensity irradiation within a Penn PhD M2 photoreactor over 96 h to reach completion (entry 12).

We then sought to compare the durability and potency of CdS QDs as photoreductants relative to a selection of visible light photocatalysts for two-photon and electron-primed photoreduction via the hydrodechlorination of **1a**.<sup>11,12,19,93,94</sup> While these comparisons are not exhaustive and no comparison of different catalysts optimized under different conditions is without limitations, we did our best to account for the differences in literature conditions by testing three different reductants (TAEA, DIPEA, and NaCHO<sub>2</sub>) and taking time points at both 24 and 48 h (Table 2 and Supporting Information Figure S2). In addition, to account for the different catalyst loadings and catalyst molecular weights, we calculated total turnover number (TON) and product/catalyst w/w comparisons. 4-DPAIPN generally performed best of the tested molecular dyes under these conditions, affording an equal amount of **2a** as the QDs when TAEA was used as the reductant



(Table 2, entries and 3). However, 0.002 mol% of CdS QDs outperformed all of the tested photoredox catalysts in terms of TON, mass of product formed per mass of catalyst, and generally overall yield across the different organic reductants tested.

**Table 2. Comparison of CdS QDs with alternate two-photon catalysts**



Entry	Photocatalyst	% Yield at 24 h <sup>a</sup>	TON (per cat.)	mg pdt. / mg cat.
1	5.9 nm CdS QDs (0.002 mol%)	95	47500	33
2	4-CzIpn (10 mol%)	24	2.4	0.66
3	4-DPAIPN (10 mol%)	96	9.6	2.7
4	[Ir(dFCF <sub>3</sub> ppy) <sub>2</sub> (dtbbpy)]PF <sub>6</sub> (2 mol%)	54	27	5.3
5	PDI (10 mol%)	16	1.6	0.59

<sup>a</sup> Corrected GC-FID yields vs. *n*-dodecane as internal standard. For experimental details, see Supporting Information Figure S2.

Intrigued by the superiority of TAEA to other amine reductants, we conducted experiments to determine whether TAEA was interacting with the QD surface. As expected for primary amines,<sup>95–97</sup> NMR experiments demonstrate that TAEA can displace the native oleate ligands from the QD surface (Figure 2 and Supporting Information Figure S3).<sup>64,65,98</sup> Based on studies of other polydentate and primary amines, TAEA presumably chelates surface-bound Cd(oleate)<sub>2</sub> complexes present on as-synthesized QDs, removing them from the QD and subsequently binding as an L-type ligand to newly exposed Cd sites on the CdS core, yielding TAEA-capped QDs.<sup>99,100</sup> Reducing the steric profile of QD ligands has been shown to improve the rate of redox

events between QDs and redox partners due to enhanced permeability of the ligand shell,<sup>73,101</sup> so one role of TAEA may be to increase surface accessibility of the QDs relative to the larger native oleate ligands. Swapping TAEA for non-coordinating DIPEA generally allowed for similar yields after 24-48 h but resulted in an induction period (>6 h) and less reproducible yields between QD batches (Table 1, entry 4 and Supporting Information Figure S4).

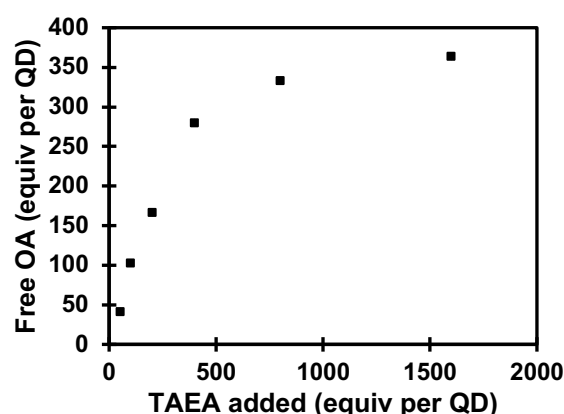


**Figure 2.** Displacement of oleate (OA) from the surface of CdS QDs ( $6 \times 10^{-6}$  mmol) after treatment with TAEA in toluene-*d*8. See Supporting Information Figure S3 for experimental details.

We hypothesize that without TAEA or other added ligands in solution, native oleate ligands slowly desorb from the QD surface under the reaction conditions, a process that occurs spontaneously in dilute QD solutions<sup>102</sup> and after negative charging of the QD<sup>103</sup> which may be faster or slower between QD batches depending upon variation in exact surface chemistry.<sup>99</sup> When using DIPEA as reductant, ligand desorption may be required for substrate or reductant access to the surface,<sup>104</sup> accounting for the observed induction period when using DIPEA. Interestingly, lowering the quantity of TAEA from 4 equivalents to 1.5 equivalents substantially increased the rate of product formation allowing for higher yields (Table 1, entries 1 and 2), while the opposite effect was observed for DIPEA (Supporting Information Figure S1),

indicating that larger excesses of TAEA may reduce substrate access to the QD surface via competitive surface association.<sup>36,48,105</sup>

**Mechanistic studies.** We conducted a series of studies to shed light on the mechanism by which CdS QDs catalyzed aryl chloride photoreductions significantly beyond their reduction potentials. We considered five main mechanisms for the reduction of **1a** (Figure 3): (A) chloride abstraction by aminoalkyl radicals generated in situ from oxidation of TAEA; (B) reduction of **1a** by a photoexcited neutral QD; (C) reduction of **1a** by a ground-state anionic QD; (D) reduction of **1a** by a hot electron generated by Auger recombination; and (E) reduction of **1a** by a hot electron generated by direct photoexcitation of a  $1S_e$  or a surface-trapped electron to a higher excited state. In the case of mechanisms B-E involving electron transfer to **1a**, the product is formed following rapid fragmentation of the nascent radical anion to afford an aryl radical which forms product after hydrogen atom transfer from solvent or reductant.

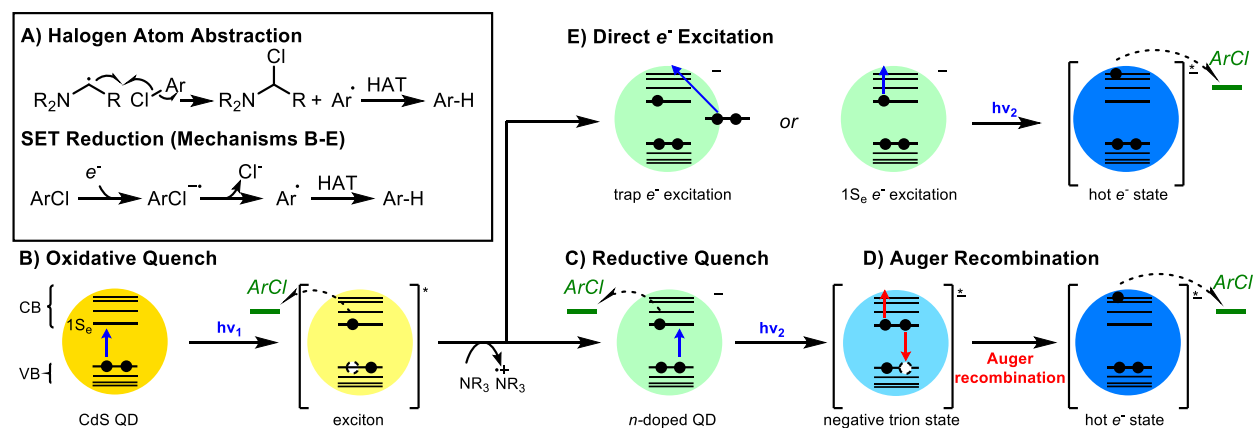


**Figure 3.** Mechanistic possibilities for aryl chloride reduction. A: Halogen atom abstraction by organic radicals derived from the reductant. B: Reduction of substrate by a neutral excited QD. C: Reduction of substrate by a ground-state anionic QD after reductive quenching. D: Reduction of substrate by a hot electron generated via Auger recombination of a negative trion state. E:

Reduction of substrate by a hot electron generated via direct excitation of electrons in the  $1S_e$  state or surface trap states.

**Mechanism A. Halogen atom transfer.** Our findings are inconsistent with a halogen atom transfer mechanism: we observed that alkyl radicals, generated using the procedure of Leonori from TAEA and sodium persulfate, did not convert **1a** to **2a** (Supporting Information Figure S5).<sup>106,107</sup> This is consistent with Leonori's findings that aryl chlorides are recalcitrant to halogen abstraction by this mechanism. Furthermore, we found that sodium formate could replace TAEA as a terminal reductant affording the product in nearly identical yield (Table 1, entries 2 and 5). The product of formate oxidation ( $\text{HCOO}^\bullet$ ) is known to undergo rapid reaction with excess formate to produce  $\text{CO}_2^{\bullet-}$ , which has been used as an SET reductant for aryl chlorides.<sup>12,108</sup> While  $\text{CO}_2^{\bullet-}$  is a strong reducing agent ( $E_{\text{red}} = -2.2 \text{ V vs. SCE}$ ),<sup>109</sup> it is incapable of reducing substrates with more negative reduction potentials than  $-2.1 \text{ vs. SCE}$ .<sup>12,108</sup> This is consistent with a QD-mediated SET reduction mechanism, regardless of reductant choice.<sup>110–112</sup>

**Mechanism B. Oxidative quenching mechanism.** Our findings are inconsistent with an oxidative quenching mechanism. That mechanism would require the excited-state QD to directly donate an electron to **1a** (Figure 3B), but Stern-Volmer quenching studies indicate that aryl chloride **1a** did not quench the PL (i.e., **1a** is not reduced by the excited state of the neutral QD). Instead, TAEA was found to quench the photoluminescence (PL) of neutral QDs (Supporting Information Figure S6). QD surface modification by TAEA is unlikely to be responsible for the observed PL quenching, because Z-type displacement of  $\text{Cd(oleate)}_2$  from the QD surface by primary amines is accompanied by amine coordination to exposed Cd sites, which enhances the QD PL. Therefore, the observed PL quenching by TAEA indicates a reductive quenching

mechanism. This rules out oxidative quenching by **1a** as in mechanism B, and suggests the intermediacy of anionic QDs (Mechanisms C-E in Figure 3).

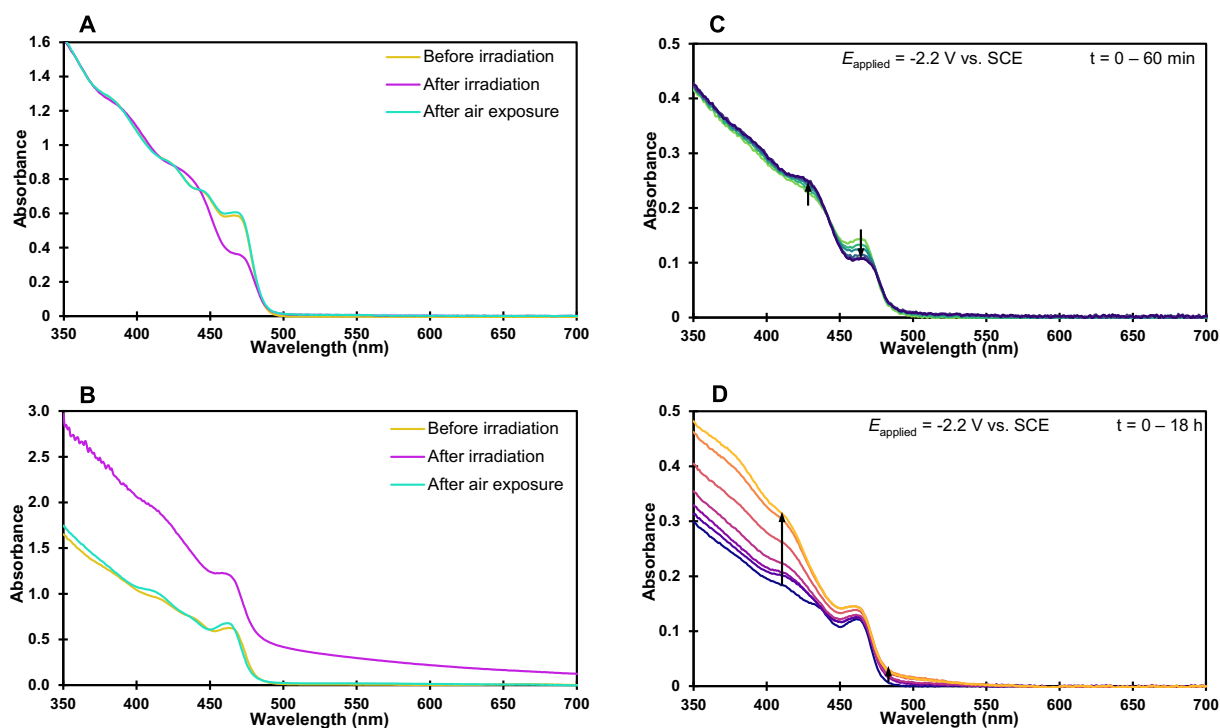


**Figure 4.** A: Air-reversible photodoping of CdS QDs in toluene by DIPEA (1000 equiv per QD) B: UV-vis spectra of catalytic reaction mixture C: Absorbance changes during reduction of CdS QDs;  $t = 0$  min (light green) to 60 min (dark blue). D: Absorbance changes during reduction of CdS QDs;  $t = 0$  h (dark purple) to 18 h (light orange).

**Mechanisms C-E. Intermediacy of anionic QDs.** Mechanisms C-E require the generation of charged QDs that are stable long enough to react with **1a** (Mechanism C) or to absorb a second photon (Mechanisms D and E). We were able to generate stable populations of anionic photodoped QDs by irradiation in the presence of catalytically competent amine reductants or  $\text{LiBHEt}_3$ <sup>70,113</sup> under air-free conditions (Figure 4A and Supporting Information Figure S7), demonstrating the feasibility of these three mechanisms. These charged QDs display bleaching of the two lowest energy excitonic features centered at 464 and 448 nm due to occupation of the

$1S_e$  electron state at the conduction band (CB) edge.<sup>114</sup> Spectral changes at higher-energy transitions were also visible, as consistent with literature reports of doped CdS QDs.<sup>115</sup> These photodoped QDs displayed similar spectral changes to those prepared using the established chemical reduction with Na/biphenyl (Supporting Information Figure S8).<sup>116</sup> The anionic QDs were stable under nitrogen and were quenched by introduction of oxygen (air). We also observed reversible photodoping of QDs in the absence of reductant, consistent with recent findings that CdS QDs can become photodoped through oxidation of their capping ligands or surface-bound water molecules without added reductants.<sup>115,117</sup> While this phenomenon can be used to generate populations of reduced QDs for spectroscopic study, added chemical reductants are required for catalytic transformations. No reduction of **1a** to **2a** occurs in the absence of terminal reductant (amine or formate) because these reductant-free photodoping pathways cannot provide enough electrons to produce a measurable amount of product in the catalytic reaction (Table 1, entry 9). Additionally, we could observe the  $1S_e$ - $1P_e$  transition of the doped electron within the CB of the anionic QDs centered at  $1500\text{ cm}^{-1}$ , consistent with other reports of CdS QDs doped with electrons (Figure 5).<sup>113,116</sup>

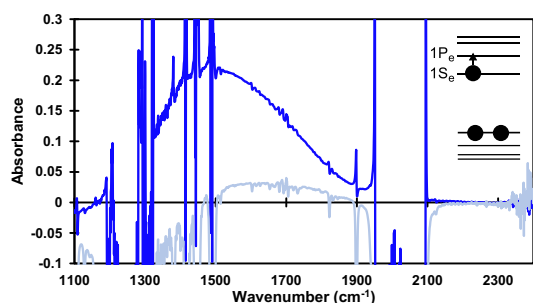


**Figure 5.** Infrared feature centered at  $1500\text{ cm}^{-1}$  formed upon photodoping of 6 nm CdS QDs, assigned to the  $1S_e$ - $1P_e$  transition of the doped electron within the conduction band. Dark blue

trace: QDs after photodoping. Light blue trace: QDs after air exposure. See Supporting Information Figure S9 for experimental details.

Slight modification of the catalytic reaction conditions to allow complete solubility of the QDs enabled UV-vis measurement of the reaction mixture to gather information about QD speciation (Figure 4B and Supporting Information Figure S10). Under irradiation with excess reductant, QDs in the catalytic reaction exhibit bleaching of the lowest energy excitonic features, consistent with photogeneration of anionic QDs. Simultaneously, the reaction mixture exhibits a broad absorbance enhancement across the entire visible spectrum (Figure 4B, pink trace), similar to spectral changes reported in core/shell ZnSe/CdS QDs after prolonged irradiation in the presence of excess DIPEA.<sup>38</sup> Absorbance tails in the visible spectrum have also been observed following chemical doping of CdSe QDs by Na/biphenyl, ascribed to the broadening and red shifting of the excitonic features by the doped electrons and excitations of electrons in surface trap states.<sup>115,118</sup> Light scattering due to QD aggregation may contribute to the broad feature, however both observed spectral changes were fully reversible after exposure to oxygen (Figure 4B, green trace), strongly suggesting that they arise from the presence of injected electrons residing in the CB (the exciton bleaching) as well as newly formed surface states (the additional broad features).<sup>103,118</sup>

To confirm the origin of these spectral changes within the catalytic reaction, we undertook spectroelectrochemistry studies, as previously employed to study CdSe nanocrystals<sup>67,119,120</sup> and deeply reducing photocatalytic systems.<sup>12,19</sup> Consistent with reports of CdS band positions, we found that cathodic reduction of 5.9 nm CdS QDs at -2.2 V vs. SCE was sufficient to electrochemically dope the QDs with ~0.5 electrons per QD within 1 h (based on the magnitude of absorbance bleaching of the 1S<sub>e</sub> feature at 464 nm),<sup>70</sup> mirroring exactly the spectral changes

observed in photodoping experiments (Figure 4C, , green to dark blue traces and Supporting Information Figure S11). The excitonic bleaching was accompanied by shifting of the higher energy absorbance features as observed in photodoped QDs (compare to Figure 4A).

When the experiment was repeated at a longer time scale, the excitonic bleaching was accompanied by a sub-band gap absorbance tail as well as further shifting and broadening of QD features between 350 and 450 nm throughout the electrolysis (Figure 4D, purple to orange traces), increasing in intensity over time, resembling the spectral changes previously observed in the catalytic reaction (Figure 4B). Sub-bandgap absorbance tails in the visible in good agreement with those observed in our experiments (Figure 4D) have been documented in spectroscopic studies of other reduced Cd-based QDs.<sup>103,113,116,118,121–123</sup> They are commonly attributed to the spontaneous reduction of surface sites (namely Cd<sup>2+</sup> ions in Cd-rich QDs) by electrons in the 1S<sub>e</sub> state, or directly by the reducing agent.<sup>103,124</sup> Reduction of the QD surface atoms leads to the introduction of surface-localized trap states filled with electrons with energy levels inside the band gap.<sup>103,125</sup> The presence of electrons in surface states introduces localized dipoles that interact with the polarizable QD exciton via the Stark effect, causing broadening of excitonic absorbance and PL features<sup>126,127</sup> when QDs are reduced by various means, potentially contributing to the observed absorbance tail. Doped electrons within the 1S<sub>e</sub> state or surface states may also exhibit transitions to higher energy states within the CB which could contribute to the observed features,<sup>103,118,123</sup> however the infrared feature corresponding to the 1S<sub>e</sub>-1P<sub>e</sub> transition (Figure 5) occupies most of the oscillator strength of the doped 1S<sub>e</sub> electrons.<sup>118</sup>

These studies strongly suggest that sequential photodoping cycles<sup>128</sup> during the catalytic reaction generate QDs with populations of electrons in the 1S<sub>e</sub> state and nascent mid-gap surface states which may form due to in-situ QD surface modification.<sup>124,129</sup> We observed that the QD



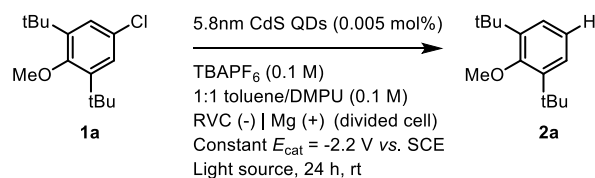
solutions remained optically clear throughout the spectroelectrochemistry experiments and note that electrolysis-induced shifts in the QD absorbance features do not resemble wavelength-dependent Rayleigh scattering (scattering cross section  $\propto \lambda^{-4}$ ), suggesting that light scattering did not majorly convolute the absorbance spectra (see Supporting Information Figure S11 for images of QDs during the experiments).

**Mechanism C. Direct reduction of 1a by anionic QDs.** Our findings are inconsistent with reduction of **1a** by anionic QDs without additional photon energy (Mechanism C). Electron-primed photoredox catalysis was used to decouple QD doping from photoexcitation.<sup>14,15,19</sup> We found that reactions utilizing a sacrificial anode (Mg(+)/RVC(-), -2.2 V vs. SCE), instead of organic reductants, formed product **2a** only when both QDs and light were present (Table 3, entries 1-3). We also observed further evidence that TAEA is serving as both a reductant and QD-stabilizing ligand:<sup>130</sup> QD decomposition could be observed over the course of the experiments, resulting in diminished yields relative to the ordinary photocatalytic reaction (Table 1, entry 1 vs Table 3, entry 1). These results demonstrate that anionic QDs must be photoexcited to reduce **1a**, ruling out mechanism C and implicating the generation of hot electrons higher in energy than the CB 1S<sub>e</sub> state.

**Mechanisms D and E. Hot electron mechanisms.** Our photodoping and spectroelectrochemistry studies established that modification of the QD surface in tandem with continuous electron injection into QDs results in a population of electrons in the 1S<sub>e</sub> state as well as surface-localized trap states, resulting in excitonic bleaching and an absorbance tail. To determine whether selective excitation of the absorbance tail could induce product formation, we employed electron-primed photocatalysis using a 525 nm light source with a 500 nm long-pass filter to selectively irradiate the absorbance tail not present in the neutral QDs, leading to small

amounts of product formation (Table 3, entry 4), consistent with the low absorbance of the doped QDs at >500 nm wavelengths. Finally, employing a 650 nm light source led to zero product formation (Table 3, entry 5), due to the negligible absorbance of QDs at red wavelengths under an applied potential of -2.2 V vs. SCE. At present we cannot rule out the possibility that direct excitation of  $1S_e$  electrons or surface electrons to high energy states contribute to the observed absorbance changes, which could contribute to the formation of hot electrons, however our results are most consistent with a dominant Auger mechanism (vide infra).

**Table 3. Electron-Primed Photoredox Studies.**



Entry	Conditions	Yield of <b>2a</b> <sup>a</sup>
1	456 nm LED lamp	65%
2	456 nm LED lamp, no QDs	0%
3	no light	0%
4	525 nm LED lamp <sup>b</sup>	9%
5	650 nm LED lamp	0%

<sup>a</sup> Corrected GC yield for reactions with 0.2 mmol **1a**. Average power consumption of LED lamps was 50 W. See Supporting Information for experimental details. <sup>b</sup> 500 nm long-pass filter employed to prevent overlap with neutral exciton.

**Mechanism D. Evidence for Auger recombination from PL measurements.** We conducted steady state and time-resolved photoluminescence measurements which demonstrate that Auger recombination (Mechanism D) occurs following irradiation of photodoped anionic CdS QDs, which form under our catalytic conditions. We observe drastic steady-state PL quenching of QD

samples following photodoping by amine reductants (Figure 6A and Supporting Information Figure S12), which was partially reversible after air exposure, a finding previously assigned to efficient Auger recombination in similar photodoped anionic QDs.<sup>113</sup> Analysis of time-resolved PL decay of QDs before and after photodoping (Figure 6B) shows multiexponential decay in all QD samples, consistent with other reports of CdS QDs (Supporting Information Figure S13).<sup>115</sup> Before photodoping, the QD sample exhibited decay components of  $\tau \sim 16$  ns, assigned to radiative decay lifetimes measured in similar QDs, as well as faster decay components of  $\tau \sim 1$  ns. After photodoping, the  $\tau \sim 16$  ns component is nearly eliminated, resulting in an approximate threefold decrease in the average PL lifetime of the nanocrystals (see Supporting Information Figure S13 for fitting data). This is indicative of Auger recombination: anionic QDs exhibit shorter fluorescent lifetimes than neutral QDs because nonradiative Auger recombination of negative trion excited states occurs more rapidly than fluorescent decay, effectively outcompeting fluorescence in photodoped QDs. After oxygen exposure, partial recovery of the neutral PL decay kinetics is observed, due to partial scavenging of electrons from doped CdS states, while surface-modification of the nanocrystals may prevent full recovery of the initial PL dynamics. Our PL data are fully consistent with reported indications of Auger recombination in photodoped QDs,<sup>71,113,115</sup> demonstrating the occurrence of this mechanism under our conditions.

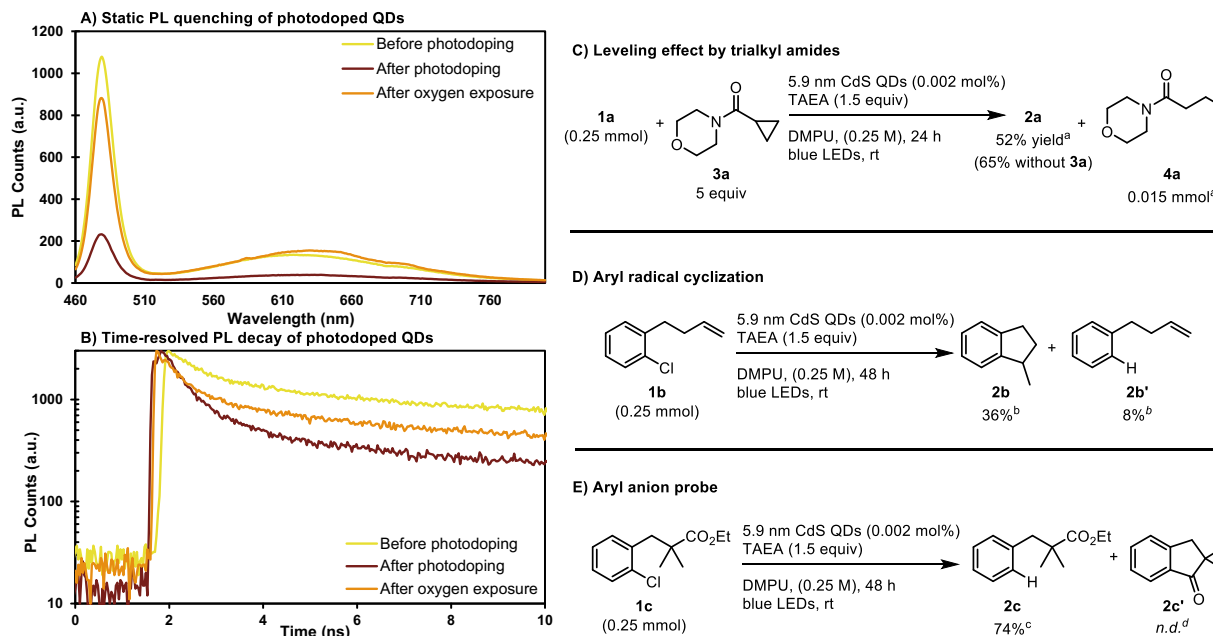


**Figure 6.** A) PL quenching in photodoped CdS QDs. B) Time-resolved PL decay of photodoped CdS QDs. C) Inhibition of reduction by amides. D) Cyclization of radical clock E) Probe for over-reduction of aryl radicals to anions. <sup>a</sup> Corrected GC-FID yields *vs.* *n*-dodecane. <sup>b</sup> <sup>1</sup>H NMR yields *vs.* CH<sub>2</sub>Br<sub>2</sub>. <sup>c</sup> Isolated yield. <sup>d</sup> No indanone cyclization product was detected via SFC-MS.

**Potential role of DMPU solvent.** The inferior performance of amide solvents and other aprotic solvents relative to DMPU led us to consider that a solvent reduction mechanism could be operative (e.g., formation of DMPU<sup>•-</sup> or DMA<sup>•-</sup>, species that have been observed when alkali metals are dissolved in these solvents)<sup>131,132</sup> and that this could impose a leveling effect on the potentials accessible by the QDs/TAEA system. The different performance would arise from differences in the reducing power of the respective radical anions because ureas like DMPU are harder to reduce to the corresponding radical anion than other carbonyl derivatives.<sup>133–135</sup> To explore this possibility, we tested the photoreduction of **1a** using DMPU as solvent in the presence of amide **3a**, which we reasoned could act as a probe for the reduction of amides to amidyl radical anions. We found that the addition of **3a** reduced the yield of dehalogenation

product **2a**, while 0.015 mmol (6 mol% relative to **1a**) of ring-opened amide **4a** was formed. (Figure 6C, Supporting Information Figure S14). While we cannot state with certainty that DMPU radical anions play a role in productive chemistry, these results demonstrate that tertiary amides can be reduced to the corresponding radical anion and inhibit productive catalysis.

**Aryl radical and aryl anion probe substrates.** While the dehalogenation reactions were assumed to arise from aryl radicals and hydrogen atom transfer, an alternative mechanism would be sequential reduction to form an aryl anion followed by proton transfer. Aryl radicals are easier to reduce than aryl halides ( $E_{\text{red}} = +0.05$  V vs. SCE for phenyl radical), so we considered that multiply charged QDs could potentially reduce aryl radicals to anions, as has been observed under electrochemical reduction conditions.<sup>136</sup> To differentiate these two mechanisms, we examined the products formed from reactions with radical clock substrate **1b** in the QDs/TAEA system (Figure 6D, Supporting Information Figure S15). The cyclized product **2b** was observed in a 4.5:1 ratio to the uncyclized olefin **2b'**, consistent with the formation and facile cyclization of aryl radicals from **1b** ( $k_{\text{cyc}} = 5 \times 10^8$  s<sup>-1</sup> at 25 °C). Recognizing that the uncyclized product could arise either by reduction of intermediate aryl radicals to the corresponding anion followed by protonation, or by HAT from solvent or reductant molecules prior to cyclization, we employed **1c** as an aryl anion probe (Figure 6E).<sup>137</sup> After reduction by QDs/TAEA, **2c** was obtained as the exclusive product with no formation of the indanone product **2c'** via anionic cyclization. These results together provide strong evidence that aryl anions are not formed under the reaction conditions, and that intermediate aryl radicals are rapidly quenched via HAT from solvent or reductant molecules (pseudo-first order rate constant  $k_{\text{HAT}} \sim 1 \times 10^8$  s<sup>-1</sup>).

**Kinetic Dependence on Light Intensity.** Kinetic studies of the reaction under differing light intensity indicate an approximate rate order of 1.4 for photons, as measured by the initial rates of

reaction over the first 5 h. A ~30 min induction period is also observed, which appears to be longer with lower light intensity (Supporting Information Figure S16). Z-type surface modification of Cd chalcogenide QDs by chelating L-type multidentate ligands like TAEA proceeds to completion within a few minutes,<sup>99</sup> so the induction period is likely not due to surface modification by TAEA. Combined with the prior observation that anionic QDs accumulate in the reaction mixture through photodoping cycles, these results are consistent with buildup of the active catalyst,<sup>6</sup> multiply anionic QDs, through photodoping at the beginning of the reaction, followed by a regime of rate-limiting hot electron transfer from photoexcited anionic QDs to substrate or solvent molecules, as would be expected given the rapid relaxation rate of hot electrons to the band edge before reduction occurs.

**Proposed Mechanism.** Based on these studies, we propose the following reduction mechanism (Figure 7): neutral QDs (**I**) become negatively charged after excitation and reductive quenching by TAEA to generate anionic QDs (**II**). **II** can then absorb a second photon to generate a negative trion state (**III**), which can undergo reductive quenching by TAEA again to return to a ground state anionic QD with an additional negative charge (**II**), or undergo Auger recombination to generate a hot-electron state (**IV**), which may then relax back to (**II**) or reduce a substrate or solvent molecule to return to a neutral or anionic ground state (**I or II**). Reduced substrates then undergo subsequent fragmentation and HAT to furnish the dehalogenated product. We also expect that back electron-transfer from reduced substrate or solvent molecules to QDs may occur competitively with productive chemistry.

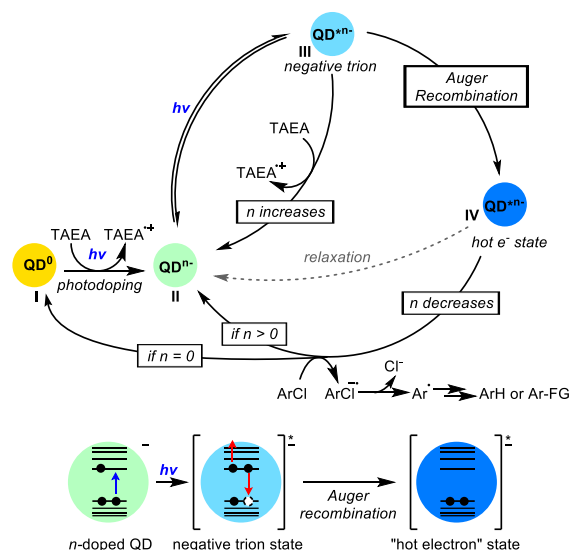
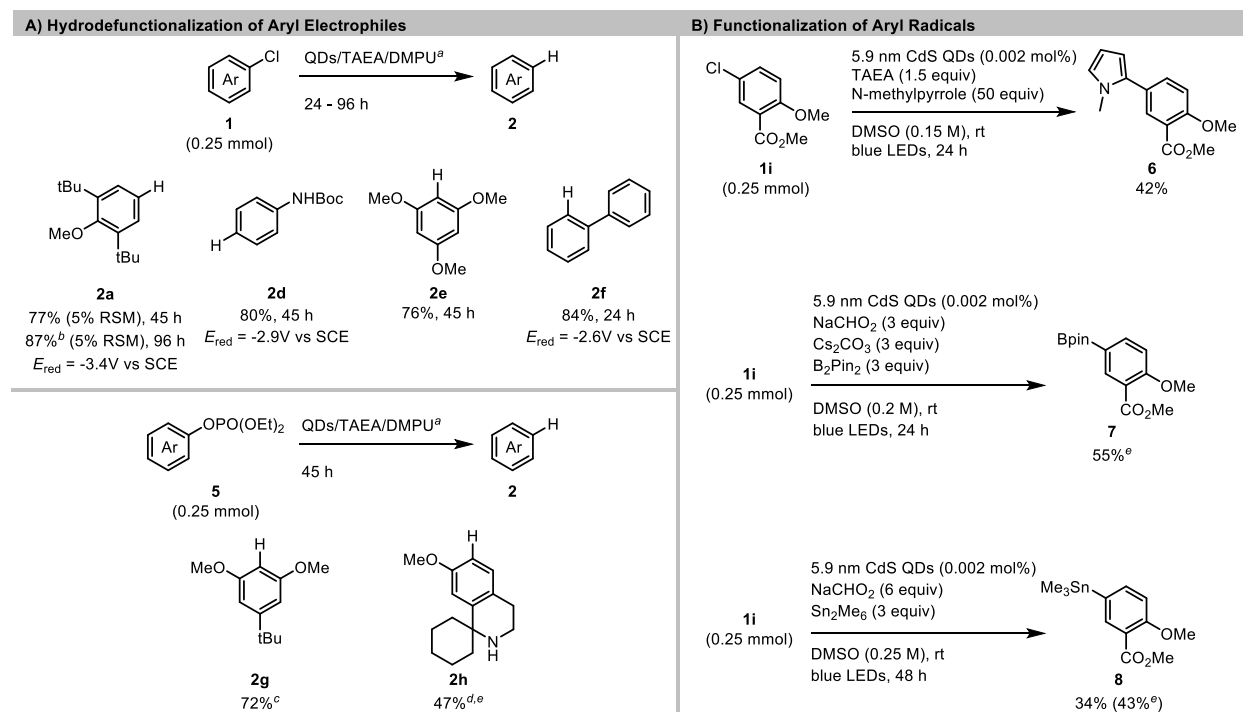


**Figure 7. Proposed mechanism of photoreduction.**

**Application to organic reactions.** To explore the synthetic utility of the CdS/TAEA system, we briefly explored the generation of aryl radicals from aryl chlorides and aryl phosphate esters (Scheme 1). For the hydrodechlorination reaction (**2a**, **2d-2h**), we found that a set of electron-rich and electron-neutral aryl chlorides could be hydrodehalogenated in high yields, while electron-rich aryl phosphate esters could be reductively cleaved to afford the arene in similar yields. Semiconductor QDs have been previously employed for reductive dehalogenation of aryl halides,<sup>34,38,138</sup> however these protocols have been limited to substrates with reduction potentials less negative than the reduction potential of the QDs. In our system, reductions of aryl electrophiles with reduction potentials significantly more negative than CdS QDs (-2.2 V *vs.* SCE)<sup>82</sup> proceeded in high yields. Considering that we were using an amine (TAEA) as the terminal reductant, we found it promising that a substrate bearing an oxidizable secondary amine (phosphate ester **5h**) could be defunctionalized in 47% yield. Because a variety of aliphatic amines can serve as terminal reductants (Supporting Information Figure S1), we think this suggests that TAEA pre-binding to the QD may outcompete more hindered amines.

To explore whether the aryl radicals formed could be used for C-C and C-X bond formation, we examined trapping reagents to furnish products **6**, **7**, and **8** in moderate yields, comparable to those reported using other aryl radical trapping conditions.<sup>15,24,38</sup> Consistent with the propensity of aryl radicals to undergo HAT with weak C-H bonds present on amine reductants and DMPU, we observed that employing DMSO as solvent and sodium formate as the terminal reductant for aryl radical trapping generally improved the selectivity for the desired products over hydrodehalogenation.<sup>12</sup> We anticipate that further improvements could be made with additional optimization: the use of DMSO instead of DMPU was required for selective aryl radical functionalization but led to lower conversion, especially for electron-rich aryl electrophiles.

### Scheme 1. Reaction scope for aryl radical generation.

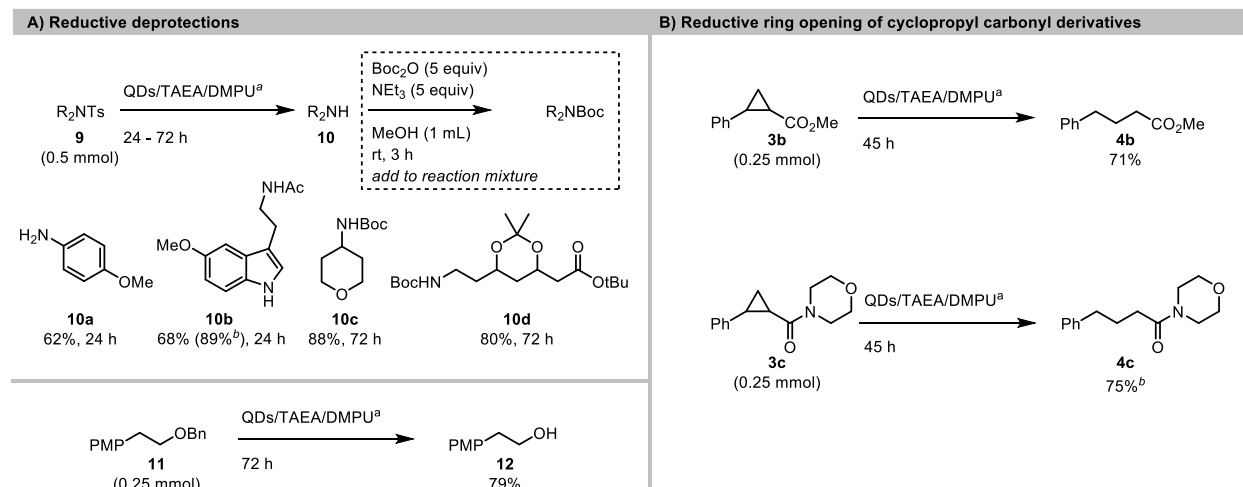


<sup>a</sup>Standard conditions used: 5.9 nm CdS QDs (0.002 mol%), TAEA (1.5 equiv), DMPU (1 mL), blue LEDs, rt. Isolated yields unless otherwise specified. <sup>b</sup>4 mmol scale, conducted in a Penn PhD M2 photoreactor (See SI for details). <sup>c</sup>DIPEA (4 equiv) used instead of TAEA. <sup>d</sup>NaCHO<sub>2</sub> (3 equiv) used instead of TAEA. <sup>e</sup>NMR yield vs. CH<sub>2</sub>Br<sub>2</sub>.



In addition to aryl radical formation from aryl chlorides, we also explored several other reductive transformations that require strong reductants (Scheme 2). The detosylation of *p*-toluenesulfonamides to amines is a common, but challenging, transformation that typically requires superstoichiometric strong reductant (e.g., SmI<sub>2</sub>,<sup>139,140</sup> Li/Naphthalene<sup>141</sup>, or Mg/MeOH<sup>142</sup>) or anhydrous strong acid (e.g., TfOH, HBr in AcOH).<sup>143</sup> Photocatalytic reductive cleavage was only recently reported using an acridinium catalyst (10 mol%) with UVA light (390 nm).<sup>93</sup> This was an exciting advance because many methods rely upon tosyl-protected nitrogen, but are of limited utility due to the harsh deprotection conditions.<sup>93</sup> In our initial examination of this reaction, several *p*-toluenesulfonamides were reductively cleaved to afford the free amines in 62-88% yield. Arylamine **9a** and melatonin-derived **9b** were completely deprotected within 24 hours, while alkylamines **9c** and **9d** were slower and required 72 h, presumably due to their more-negative reduction potentials ( $E_{\text{red}} \sim -2.4$  V vs. SCE for *N*-tosyl alkylamines),<sup>144</sup> or higher propensity for back-electron transfer before fragmentation. Notably, sulfonyl-protected phenols have been reductively deprotected using CuInS<sub>2</sub>/ZnS QDs as a photocatalyst,<sup>50</sup> however only electron-poor sulfonyl groups with reduction potentials less-negative than the employed QDs were cleaved under these conditions, in contrast to this study with CdS QDs.

## Scheme 2. Additional reductive transformations.



<sup>a</sup>Standard conditions used: 5.9 nm CdS QDs (0.002 mol%), TAEA (1.5 equiv), DMPU (1 mL), blue LEDs, rt. Isolated yields unless otherwise specified. <sup>b</sup>NMR yield vs. CH<sub>2</sub>Br<sub>2</sub>.

Besides tosylate deprotection, these conditions were also able to deprotect alkyl benzyl ether **11** to alcohol **12** in high yield. Debencylation is commonly accomplished through Pd-catalyzed hydrogenation. However, in situations where hydrogenolysis is incompatible with other substrate functionalities, it may also be accomplished by strong stoichiometric reductants<sup>145–148</sup>, electroreduction ( $E_{red} = -3.1$  V vs. SCE)<sup>144</sup>, or the combination of an organic reductant and UV light.<sup>149</sup> This approach allows clean deprotection to proceed under visible light irradiation with amine terminal reductants.

Finally, the reductive C-C bond cleavage of cyclopropyl ester **3b** and amide **3c** bearing beta phenyl groups could be achieved in high yield via reduction of the ester ( $E_{red} = -2.8$  V vs SCE)<sup>150</sup> or amide<sup>151</sup> functionalities to the corresponding ketyl radical anion, followed by ring-opening to afford the distal benzylic radical anion. While the reductive ring opening of aryl cyclopropyl ketones is well-known in photoredox catalysis<sup>152–154</sup> ( $E_{red} = -2.10$  V vs SCE for phenyl cyclopropyl ketone),<sup>155</sup> only one example exists of a photocatalyzed reductive ring opening of a more electron-rich cyclopropane carboxylic acid.<sup>13</sup> Reductive ring openings of the analogous

cyclopropanecarboxyl esters and amides have only been achieved by employing excess  $\text{SmI}_2$  activated by  $\text{H}_2\text{O}$ , where care must be taken to avoid over-reduction to the alcohol.<sup>156</sup> Reductive ring openings of cyclopropyl ketones have enabled many valuable transformations including mono<sup>157</sup> and di-functionalizations,<sup>152,153,158–164</sup> so we anticipate that further development of these ester and amide ring opening protocols will enable more complex transformations.

## Discussion

**Evidence for an Auger Recombination Mechanism.** Our findings are most consistent with a dominant Auger mechanism for hot electron generation. Spectral measurement of our CdS QDs after doping procedures and under various reaction conditions are consistent with the in-situ generation of anionic QDs with electron occupation of the  $1\text{S}_e$  state and surface states. After photochemical or electrochemical doping of QDs, the excitonic feature of the reduced QDs accounts for most of the absorbance of the reaction mixture at blue wavelengths. Excitation of anionic QDs produces negative trion states which are known to efficiently undergo Auger recombination, generating hot electrons. This was confirmed by our ex-situ photoluminescence studies of anionic CdS QDs, which were consistent with literature reports of anionic QDs undergoing Auger recombination,<sup>70,115</sup> demonstrating the intermediacy of this process within our system. Importantly, surface modification of QDs and the introduction of electrons in trap states, which occur under our reaction conditions, do not interfere with Auger recombination events.<sup>75,165,166</sup> While the exact degree of negative charging of the QDs under purely photochemical conditions remains unknown, excited QDs with multiple negative charges are known to undergo Auger recombination faster than monoanionic QDs and produce longer-lived hot electrons.<sup>165</sup> We propose that Auger recombination to generate hot electrons could reasonably happen from a variety of anionic QD species that may be present in the reaction. Electron-primed

photoredox catalysis enabled the direct study of anionic QDs: irradiation of QDs and substrate with 456 nm light in tandem with electrochemical reduction at -2.2V *vs.* SCE leads to effective reduction of substrate **1a**, requiring QDs, light, and current to achieve any conversion. Employing >500 nm light to selectively excite the absorbance tail forms small amounts of product, showing that irradiation of this feature can also generate hot electrons. However, the low absorbance of this feature compared to the exciton of the doped QDs suggest that Auger recombination is the dominant mechanism of hot electron generation.

**Hot Electron Transfer from QDs.** A significant challenge of conPET and electron-primed photoreductions is the short-lived nature of the highly reducing excited state. Rapid unimolecular relaxation or decomposition processes of excited-state radical anions limit the efficiency of bimolecular electron transfer to substrates.<sup>21,167</sup> Indeed, the notably short lifetimes of excited state radical anions (typically on the order of ps) have raised questions about the active photoreductants in these systems.<sup>21,22</sup> A critical step of our proposed mechanism is the transfer of hot electrons from the QD to the substrate before relaxation back to the band edge state. The longest-lived hot electrons in semiconductor QDs exhibit lifetimes near 1 ns in core-shell QDs,<sup>165,168</sup> however they typically relax back to the band edge within picoseconds, depending on the QD surface chemistry.<sup>78,169–171</sup> One advantage of employing QDs in this context is their ability to bind organic molecules as ligands (up to several hundred per CdS QD). Pre-association between substrates and the QD surface can help bypass the kinetic obstacles associated with highly reducing but short-lived excited states. The ps lifetimes of hot electrons in QDs, while insufficient for efficient collisional electron transfer, are sufficiently long for electron transfer to surface-bound or nearby species.<sup>78,80,172</sup> While many of the substrates used in this study do not contain functional groups commonly used as strongly-binding QD ligands, many classes of

weakly coordinating molecules, including solvent, may transiently associate with the QD surface through dispersion, electrostatic, or other noncovalent interactions.<sup>48,105,130</sup> In principle, this would allow the observed reductions to take place through ultrafast charge transfer to the adsorbed substrate competitive with hot electron cooling.

**Potential of QDs for Reductive Chemistry.** These studies demonstrate that semiconductor quantum dots hold promise as versatile, robust visible light photoredox catalysts for strong reductions. The potentials accessible are already strong enough to be competitive with the best available catalysts (Table 2), and the total turnover numbers for the catalysts are an order of magnitude better than previously reported for visible light photoreductions of electron-rich aryl chlorides. The generality of this catalyst is also beneficial; one quantum dot (5.8-6.0 nm oleate-capped CdS QDs) worked for a variety of reactions (hydrodefunctionalization, heteroarylation, borylation, and stannylation of aryl chlorides; deprotection of tosyl-protected amines and benzyl-protected alcohols, and ring-opening of cyclopropanecarboxylate derivatives). While the MW of these CdS QDs is high (approximately 330 kDa of CdS and 140 kDa of oleic acid ligands for 6.0 nm CdS QDs), *their productivity is high even on a mass product/mass QD scale* (Table 2 and Supporting Information Figure S2). In contrast to most other small molecule dyes, CdS QDs are made in a single step process that does not require chromatography from materials that are very low cost (approximately \$13 USD per gram of isolated QDs based on material costs for the described synthesis; ~2 mg of QDs are used per 0.25 mmol-scale reaction). At the end of the reaction, QDs can be easily removed from reaction media via precipitation, filtration through silica, or dissolution in acid. Although cadmium is tightly regulated in drug products, we found previously that precipitation of CdSe QDs, with or without additional purification, leads to amounts of Cd in the product that are within allowed limits.<sup>34</sup> Together, these results demonstrate

how simple colloidal nanoparticles can offer advantages over small molecule molecular dyes. Looking towards the future, tailored nanomaterials optimized for catalytic performance are likely to perform even better, new materials with lower toxicity could be explored for organic chemistry,<sup>173</sup> and surface association could be further exploited for selectivity.<sup>25,37,105</sup>

## Conclusions

We have demonstrated the potential of CdS QDs with mild organic reductants and visible light (450 nm) to function as strong photoreductants for a variety of organic transformations which require strong reducing agents. Mechanistic studies implicate a similar process to reported conPET mechanisms, wherein neutral QDs become negatively charged through excitation and reductive quenching by the terminal organic reductant. Hot electrons are then generated via excitation of the anionic QDs and subsequent Auger recombination of the negative trion state. Advantages of this approach include the ease of catalyst synthesis and the high stability of CdS QDs under strongly reducing conditions, with turnover numbers of up to 47500 (per QD) achieved under photochemical conditions or 13000 for electron-primed photoredox catalysis. Further explorations of reductive transformations catalyzed by CdS QDs will be reported in due course.

## ASSOCIATED CONTENT

**Supporting Information.** Additional optimization and characterization data, experimental procedures, and characterization data for all isolated compounds (PDF) This material is available free of charge via the Internet at <http://pubs.acs.org>.

## AUTHOR INFORMATION

### Corresponding Authors

Daniel J. Weix - Department of Chemistry, University of Wisconsin-Madison, Madison,  
Wisconsin 53706, United States. ORCID: <https://orcid.org/0000-0002-9552-3378>

Email: [dweix@wisc.edu](mailto:dweix@wisc.edu)

## **Authors**

Jonas K. Widness - Department of Chemistry, University of Wisconsin-Madison, Madison,  
Wisconsin 53706, United States. ORCID: <https://orcid.org/0000-0002-7507-8254>

Daniel G. Enny - Department of Chemistry, University of Wisconsin-Madison, Madison,  
Wisconsin 53706, United States. ORCID: <https://orcid.org/0000-0002-8644-4694>

Kaelyn S. McFarlane-Connelly - Department of Chemistry, University of Rochester,  
Rochester, New York 14586, United States. ORCID: <https://orcid.org/0000-0002-6522-2064>

Mahilet T. Miedenbauer – Materials Science Program, University of Rochester, Rochester,  
New York 14586, United States. ORCID: <https://orcid.org/0000-0001-8085-7167>

Todd D. Krauss - Department of Chemistry, University of Rochester, Rochester, New York  
14586, United States. ORCID: <https://orcid.org/0000-0002-4860-874X>

## **Funding Sources**

### **ACKNOWLEDGMENT**

This work was supported by the NIH (R21GM141622 to DJW and TDK), the NSF (CHE-1904847 to TDK), the University of Wisconsin-Madison (DJW), and the donors to the Wayland E. Noland Chair (DJW). The instrumentation in the PBCIC was supported as follows: Thermo Q Extractive Plus was supported by the NIH (No. 1S10 OD020022); Shimadzu GCMS-QP2010S was supported by the Department of Chemistry; Bruker Avance III 500 was supported by a generous gift from Paul J. and Margaret M. Bender. We thank the entire Wickens and Yoon groups (UW-Madison) for access to their chemical inventories, Colleen Chernowsky (UW-Madison) for assistance with electron-primed photoredox catalysis, and the Stahl group (UW-Madison) for access to UV-vis instrumentation. We thank Dr. Alina Schimpf (University of California San Diego) for helpful discussions about FTIR measurements.

### **REFERENCES**

- (1) Romero, N. A.; Nicewicz, D. A. Organic Photoredox Catalysis. *Chem. Rev.* **2016**, *116*, 10075–10166.
- (2) Yoon, T. P.; Ischay, M. A.; Du, J. Visible light photocatalysis as a greener approach to photochemical synthesis. *Nat. Chem.* **2010**, *2*, 527–532.
- (3) Glaser, F.; Wenger, O. S. Recent progress in the development of transition-metal based photoredox catalysts. *Coord. Chem. Rev.* **2020**, *405*, 213129.
- (4) Mdluli, V.; Diluzio, S.; Lewis, J.; Kowalewski, J. F.; Connell, T. U.; Yaron, D.; Kowalewski, T.; Bernhard, S. High-throughput Synthesis and Screening of Iridium(III) Photocatalysts for the Fast and Chemoselective Dehalogenation of Aryl Bromides. *ACS Catal.* **2020**, *10*, 6977–6987.
- (5) Qiao, Y.; Schelter, E. J. Lanthanide Photocatalysis. *Acc. Chem. Res.* **2018**, *51*, 2926–2936.
- (6) Glaser, F.; Kerzig, C.; Wenger, O. S. Multi-Photon Excitation in Photoredox Catalysis: Concepts, Applications, Methods. *Angew. Chem. Int. Ed.* **2020**, *59*, 10266–10284.
- (7) Prier, C. K.; Rankic, D. A.; MacMillan, D. W. C. Visible Light Photoredox Catalysis with Transition Metal Complexes: Applications in Organic Synthesis. *Chem. Rev.* **2013**, *113*, 5322–5363.
- (8) Speck, F.; Rombach, D.; Wagenknecht, H.-A. N-Arylphenothiazines as strong donors for photoredox catalysis – pushing the frontiers of nucleophilic addition of alcohols to alkenes. *Beilstein J. Org. Chem.* **2019**, *15*, 52–59.
- (9) Discekici, E. H.; Treat, N. J.; Poelma, S. O.; Mattson, K. M.; Hudson, Z. M.; Luo, Y.; Hawker, C. J.; de Alaniz, J. R. A highly reducing metal-free photoredox catalyst: design and application in radical dehalogenations. *Chem. Commun.* **2015**, *51*, 11705–11708.
- (10) Shaw, M. H.; Twilton, J.; MacMillan, D. W. C. Photoredox Catalysis in Organic Chemistry. *J. Org. Chem.* **2016**, *81*, 6898–6926.
- (11) Ghosh, I.; Ghosh, T.; Bardagi, J. I.; König, B. Reduction of aryl halides by consecutive visible light-induced electron transfer processes. *Science* **2014**, *346*, 725.
- (12) Chmiel, A. F.; Williams, O. P.; Chernowsky, C. P.; Yeung, C. S.; Wickens, Z. K. Non-innocent Radical Ion Intermediates in Photoredox Catalysis: Parallel Reduction Modes Enable Coupling of Diverse Aryl Chlorides. *J. Am. Chem. Soc.* **2021**, *143*, 10882–10889.
- (13) Cole, J. P.; Chen, D.-F.; Kudisch, M.; Pearson, R. M.; Lim, C.-H.; Miyake, G. M. Organocatalyzed Birch Reduction Driven by Visible Light. *J. Am. Chem. Soc.* **2020**, *142*, 13573–13581.
- (14) Cowper, N. G. W.; Chernowsky, C. P.; Williams, O. P.; Wickens, Z. K. Potent Reductants via Electron-Primed Photoredox Catalysis: Unlocking Aryl Chlorides for Radical Coupling. *J. Am. Chem. Soc.* **2020**, *142*, 2093–2099.
- (15) Kim, H.; Kim, H.; Lambert, T. H.; Lin, S. Reductive Electrophotocatalysis: Merging Electricity and Light To Achieve Extreme Reduction Potentials. *J. Am. Chem. Soc.* **2020**, *142*, 2087–2092.
- (16) Liu, J.; Lu, L.; Wood, D.; Lin, S. New Redox Strategies in Organic Synthesis by Means of Electrochemistry and Photochemistry. *ACS Cent. Sci.* **2020**, *6*, 1317–1340.
- (17) Cabby, S.; Bouchet, L. M.; Argüello, J. E.; Rossi, R. A.; Bardagi, J. I. Excitation of Radical Anions of Naphthalene Diimides in Consecutive- and Electro-Photocatalysis\*\*. *ChemCatChem* **2021**, *13*, 3001–3009.



- (18) Chen, Y.-J.; Lei, T.; Hu, H.-L.; Wu, H.-L.; Zhou, S.; Li, X.-B.; Chen, B.; Tung, C.-H.; Wu, L.-Z. Tandem photoelectrochemical and photoredox catalysis for efficient and selective aryl halides functionalization by solar energy. *Matter* **2021**, *4*, 2354–2366.
- (19) Chernowsky, C. P.; Chmiel, A. F.; Wickens, Z. K. Electrochemical Activation of Diverse Conventional Photoredox Catalysts Induces Potent Photoreductant Activity\*\*. *Angew. Chem. Int. Ed.* **2021**, *60*, 21418.
- (20) The highest catalyst TONs for reductive conPET and electron-primed photoredox procedures proceeding via photoexcitation of in-situ generated photocatalyst radical anions are ~100 for organocatalysts and ~3000 for Ru-based dyes. See: (a) Bell, J. D.; Murphy, J. A. Recent Advances in Visible Light-Activated Radical Coupling Reactions Triggered by (i) Ruthenium, (ii) Iridium and (iii) Organic Photoredox Agents. *Chem. Soc. Rev.* **2021**, *50*, 9540–9685. (b) Glaser, F.; Kerzig, C.; Wenger, O. S. Multi-Photon Excitation in Photoredox Catalysis: Concepts, Applications, Methods. *Angew. Chem. Int. Ed.* **2020**, *59*, 10266–10284. (c) Barham, J. P.; König, B. Synthetic Photoelectrochemistry. *Angew. Chem. Int. Ed.* **2020**, *59*, 11732–11747. (d) Liu, J.; Lu, L.; Wood, D.; Lin, S. New Redox Strategies in Organic Synthesis by Means of Electrochemistry and Photochemistry. *ACS Cent. Sci.* **2020**, *6*, 1317–1340. (e) Naumann, R.; Lehmann, F.; Goetz, M. Micellized Tris(Bipyridine)Ruthenium Catalysts Affording Preparative Amounts of Hydrated Electrons with a Green Light-Emitting Diode. *Chem. – Eur. J.* **2018**, *24*, 13259–13269.
- (21) Rieth, A. J.; Gonzalez, M. I.; Kudisch, B.; Nava, M.; Nocera, D. G. How Radical Are “Radical” Photocatalysts? A Closed-Shell Meisenheimer Complex Is Identified as a Super-Reducing Photoreagent. *J. Am. Chem. Soc.* **2021**, *143*, 14352–14359.
- (22) Marchini, M.; Gualandi, A.; Mengozzi, L.; Franchi, P.; Lucarini, M.; Cozzi, P. G.; Balzani, V.; Ceroni, P. Mechanistic insights into two-photon-driven photocatalysis in organic synthesis. *Phys. Chem. Chem. Phys.* **2018**, *20*, 8071–8076.
- (23) White, A. R.; Wang, L.; Nicewicz, D. A. Synthesis and Characterization of Acridinium Dyes for Photoredox Catalysis. *Synlett* **2019**, *30*, 827–832.
- (24) Xu, J.; Cao, J.; Wu, X.; Wang, H.; Yang, X.; Tang, X.; Toh, R. W.; Zhou, R.; Yeow, E. K. L.; Wu, J. Unveiling Extreme Photoreduction Potentials of Donor–Acceptor Cyanoarenes to Access Aryl Radicals from Aryl Chlorides. *J. Am. Chem. Soc.* **2021**, *143*, 13266–13273.
- (25) Kodaimati, M. S.; McClelland, K. P.; He, C.; Lian, S.; Jiang, Y.; Zhang, Z.; Weiss, E. A. Viewpoint: Challenges in Colloidal Photocatalysis and Some Strategies for Addressing Them. *Inorg. Chem.* **2018**, *57*, 3659–3670.
- (26) Yuan, Y.; Jin, N.; Saghy, P.; Dube, L.; Zhu, H.; Chen, O. Quantum Dot Photocatalysts for Organic Transformations. *J. Phys. Chem. Lett.* **2021**, *12*, 7180–7193.
- (27) Bailes, J. Photostability of Semiconductor Quantum Dots in Response to UV Exposure. In *Nanoparticles in Biology and Medicine: Methods and Protocols*; Ferrari, E., Soloviev, M., Eds.; Springer US: New York, NY, 2020; pp 343–349.
- (28) Das, A.; Han, Z.; Haghighi, M. G.; Eisenberg, R. Photogeneration of hydrogen from water using CdSe nanocrystals demonstrating the importance of surface exchange. *Proc. Natl. Acad. Sci.* **2013**, *110*, 16716.
- (29) Gould, T. J.; Bewersdorf, J.; Hess, S. T. A Quantitative Comparison of the Photophysical Properties of Selected Quantum Dots and Organic Fluorophores. *Z. Für Phys. Chem.* **2008**, *222*, 833–849.

- (30) Resch-Genger, U.; Grabolle, M.; Cavaliere-Jaricot, S.; Nitschke, R.; Nann, T. Quantum dots versus organic dyes as fluorescent labels. *Nat. Methods* **2008**, *5*, 763–775.
- (31) Bruchez Marcel; Moronne Mario; Gin Peter; Weiss Shimon; Alivisatos A. Paul. Semiconductor Nanocrystals as Fluorescent Biological Labels. *Science* **1998**, *281*, 2013–2016.
- (32) Hahn, M. A.; Tabb, J. S.; Krauss, T. D. Detection of Single Bacterial Pathogens with Semiconductor Quantum Dots. *Anal. Chem.* **2005**, *77*, 4861–4869.
- (33) Urban, J. M.; Chiang, W.; Hammond, J. W.; Cogan, N. M. B.; Litzburg, A.; Burke, R.; Stern, H. A.; Gelbard, H. A.; Nilsson, B. L.; Krauss, T. D. Quantum Dots for Improved Single-Molecule Localization Microscopy. *J. Phys. Chem. B* **2021**, *125*, 2566–2576.
- (34) Caputo, J. A.; Frenette, L. C.; Zhao, N.; Sowers, K. L.; Krauss, T. D.; Weix, D. J. General and Efficient C–C Bond Forming Photoredox Catalysis with Semiconductor Quantum Dots. *J. Am. Chem. Soc.* **2017**, *139*, 4250–4253.
- (35) Huang, C.; Li, X.-B.; Tung, C.-H.; Wu, L.-Z. Photocatalysis with Quantum Dots and Visible Light for Effective Organic Synthesis. *Chem. – Eur. J.* **2018**, *24*, 11530–11534.
- (36) Zhang, Z.; Edme, K.; Lian, S.; Weiss, E. A. Enhancing the Rate of Quantum-Dot-Photocatalyzed Carbon–Carbon Coupling by Tuning the Composition of the Dot's Ligand Shell. *J. Am. Chem. Soc.* **2017**, *139*, 4246–4249.
- (37) Jiang, Y.; Wang, C.; Rogers, C. R.; Kodaimati, M. S.; Weiss, E. A. Regio- and diastereoselective intermolecular [2+2] cycloadditions photocatalysed by quantum dots. *Nat. Chem.* **2019**, *11*, 1034–1040.
- (38) Pal, A.; Ghosh, I.; Sapra, S.; Koenig, B. Quantum Dots in Visible-Light Photoredox Catalysis: Reductive Dehalogenations and C-H Arylation Reactions Using Aryl Bromides. *Chem. Mater.* **2017**, *29*, 5225–5231.
- (39) Zhang, Z.; Rogers, C. R.; Weiss, E. A. Energy Transfer from CdS QDs to a Photogenerated Pd Complex Enhances the Rate and Selectivity of a Pd-Photocatalyzed Heck Reaction. *J. Am. Chem. Soc.* **2020**, *142*, 495–501.
- (40) Hu, Q.; Yu, X.; Gong, S.; Chen, X. Nanomaterial catalysts for organic photoredox catalysis-mechanistic perspective. *Nanoscale* **2021**, *13*, 18044–18053.
- (41) Hu, J.; Pu, T.-J.; Xu, Z.-W.; Xu, W.-Y.; Feng, Y.-S. Cadmium Sulfide Quantum-Dot-Photocatalyzed Cascade Cyclization of Functionalized Difluoromethyl Chlorides with Unactivated Olefins. *Adv. Synth. Catal.* **2019**, *361*, 708–713.
- (42) Wang, D.-Y.; Yin, Y.-Y.; Feng, C.-W.; Rukhsana; Shen, Y.-M. Advances in Homogeneous Photocatalytic Organic Synthesis with Colloidal Quantum Dots. *Catalysts* **2021**, *11*, 275.
- (43) Yuan, Y.; Zhu, H.; Hills-Kimball, K.; Cai, T.; Shi, W.; Wei, Z.; Yang, H.; Candler, Y.; Wang, P.; He, J.; Chen, O. Stereoselective C–C Oxidative Coupling Reactions Photocatalyzed by Zwitterionic Ligand Capped CsPbBr<sub>3</sub> Perovskite Quantum Dots. *Angew. Chem. Int. Ed.* **2020**, *59*, 22563–22569.
- (44) Huang, C.; Qiao, J.; Ci, R.-N.; Wang, X.-Z.; Wang, Y.; Wang, J.-H.; Chen, B.; Tung, C.-H.; Wu, L.-Z. Quantum dots enable direct alkylation and arylation of allylic C(sp<sup>3</sup>)–H bonds with hydrogen evolution by solar energy. *Chem* **2021**, *7*, 1244–1257.
- (45) Qiao, J.; Song, Z.-Q.; Huang, C.; Ci, R.-N.; Liu, Z.; Chen, B.; Tung, C.-H.; Wu, L.-Z. Direct, Site-Selective and Redox-Neutral  $\alpha$ -C–H Bond Functionalization of Tetrahydrofurans via Quantum Dots Photocatalysis. *Angew. Chem. Int. Ed.* **2021**, *60*, 27201–27205.

- (46) Huang, C.; Ci, R.-N.; Qiao, J.; Wang, X.-Z.; Feng, K.; Chen, B.; Tung, C.-H.; Wu, L.-Z. Direct Allylic C(sp<sup>3</sup>)-H and Vinylic C(sp<sup>2</sup>)-H Thiolation with Hydrogen Evolution by Quantum Dots and Visible Light. *Angew. Chem. Int. Ed.* **2021**, *60*, 11779–11783.
- (47) Chai, Z.; Zeng, T.-T.; Li, Q.; Lu, L.-Q.; Xiao, W.-J.; Xu, D. Efficient Visible Light-Driven Splitting of Alcohols into Hydrogen and Corresponding Carbonyl Compounds over a Ni-Modified CdS Photocatalyst. *J. Am. Chem. Soc.* **2016**, *138*, 10128–10131.
- (48) Jensen, S. C.; Bettis Homan, S.; Weiss, E. A. Photocatalytic Conversion of Nitrobenzene to Aniline through Sequential Proton-Coupled One-Electron Transfers from a Cadmium Sulfide Quantum Dot. *J. Am. Chem. Soc.* **2016**, *138*, 1591–1600.
- (49) Jiang, Y.; Weiss, E. Colloidal Quantum Dots as Photocatalysts for Triplet Excited State Reactions of Organic Molecules. *J. Am. Chem. Soc.* **2020**, *142*, 15219–15229.
- (50) Perez, K. A.; Rogers, C. R.; Weiss, E. A. Quantum Dot-Catalyzed Photoreductive Removal of Sulfonyl-Based Protecting Groups. *Angew. Chem. Int. Ed.* **2020**, *59*, 14091–14095.
- (51) McClelland, K. P.; Weiss, E. A. Selective Photocatalytic Oxidation of Benzyl Alcohol to Benzaldehyde or C-C Coupled Products by Visible-Light-Absorbing Quantum Dots. *Acs Appl. Energy Mater.* **2019**, *2*, 92–96.
- (52) Xi, Z.-W.; Yang, L.; Wang, D.-Y.; Pu, C.-D.; Shen, Y.-M.; Wu, C.-D.; Peng, X.-G. Visible-Light Photocatalytic Synthesis of Amines from Imines via Transfer Hydrogenation Using Quantum Dots as Catalysts. *J. Org. Chem.* **2018**, *83*, 11886–11895.
- (53) Xi, Z.-W.; Yang, L.; Wang, D.-Y.; Feng, C.-W.; Qin, Y.; Shen, Y.-M.; Pu, C.; Peng, X. Visible Light Induced Reduction and Pinacol Coupling of Aldehydes and Ketones Catalyzed by Core/Shell Quantum Dots. *J. Org. Chem.* **2021**, *86*, 2474–2488.
- (54) Lei, T.; Wei, S.-M.; Feng, K.; Chen, B.; Tung, C.-H.; Wu, L.-Z. Borylation of Diazonium Salts by Highly Emissive and Crystalline Carbon Dots in Water. *ChemSusChem* **2020**, *13*, 1715–1719.
- (55) Simlandy, A. K.; Bhattacharyya, B.; Pandey, A.; Mukherjee, S. Picosecond Electron Transfer from Quantum Dots Enables a General and Efficient Aerobic Oxidation of Boronic Acids. *ACS Catal.* **2018**, *8*, 5206–5211.
- (56) Muralirajan, K.; Kancharla, R.; Bau, J. A.; Taksande, M. R.; Qureshi, M.; Takanabe, K.; Rueping, M. Exploring the Structure and Performance of Cd-Chalcogenide Photocatalysts in Selective Trifluoromethylation. *ACS Catal.* **2021**, *11*, 14772–14780.
- (57) Chakraborty, I. N.; Roy, S.; Devatha, G.; Rao, A.; Pillai, P. P. InP/ZnS Quantum Dots as Efficient Visible-Light Photocatalysts for Redox and Carbon–Carbon Coupling Reactions. *Chem. Mater.* **2019**, *31*, 2258–2262.
- (58) Li, J.; Zhao, J.; Ma, C.; Yu, Z.; Zhu, H.; Yun, L.; Meng, Q. Visible-Light-Driven Oxidative Cleavage of Alkenes Using Water-Soluble CdSe Quantum Dots. *ChemSusChem* **2021**, *14*, 4985–4992.
- (59) Chandrashekar, H. B.; Maji, A.; Halder, G.; Banerjee, S.; Bhattacharyya, S.; Maiti, D. Photocatalyzed borylation using water-soluble quantum dots. *Chem. Commun.* **2019**, *55*, 6201–6204.
- (60) Wu, X.; Xie, S.; Liu, C.; Zhou, C.; Lin, J.; Kang, J.; Zhang, Q.; Wang, Z.; Wang, Y. Ligand-Controlled Photocatalysis of CdS Quantum Dots for Lignin Valorization under Visible Light. *ACS Catal.* **2019**, *9*, 8443–8451.
- (61) Zhu, X.; Lin, Y.; San Martin, J.; Sun, Y.; Zhu, D.; Yan, Y. Lead halide perovskites for photocatalytic organic synthesis. *Nat. Commun.* **2019**, *10*, 2843.

- (62) CdS QDs are made in one step using standard benchtop synthesis techniques from CdO (\$40/mol), oleic acid (\$10/mol) and sulfur (\$1.45/mol) in octadecene (\$40/L). They are isolated by precipitation and stored as solutions in toluene. See Supporting Information for further details.
- (63) Fritzinger, B.; Capek, R. K.; Lambert, K.; Martins, J. C.; Hens, Z. Utilizing Self-Exchange To Address the Binding of Carboxylic Acid Ligands to CdSe Quantum Dots. *J. Am. Chem. Soc.* **2010**, *132*, 10195–10201.
- (64) Knauf, R. R.; Lennox, J. C.; Dempsey, J. L. Quantifying Ligand Exchange Reactions at CdSe Nanocrystal Surfaces. *Chem. Mater.* **2016**, *28*, 4762–4770.
- (65) Hens, Z.; Martins, J. C. A Solution NMR Toolbox for Characterizing the Surface Chemistry of Colloidal Nanocrystals. *Chem. Mater.* **2013**, *25*, 1211–1221.
- (66) Morozov Sergii; Pensa Evangelina L.; Khan Ali Hossain; Polovitsyn Anatolii; Cortés Emiliano; Maier Stefan A.; Vezzoli Stefano; Moreels Iwan; Sapienza Riccardo. Electrical control of single-photon emission in highly charged individual colloidal quantum dots. *Sci. Adv.* **2020**, *6*, eabb1821.
- (67) Ashokan, A.; Mulvaney, P. Spectroelectrochemistry of Colloidal CdSe Quantum Dots. *Chem. Mater.* **2021**, *33*, 1353–1362.
- (68) Harris, R. D.; Bettis Homan, S.; Kodaimati, M.; He, C.; Nepomnyashchii, A. B.; Swenson, N. K.; Lian, S.; Calzada, R.; Weiss, E. A. Electronic Processes within Quantum Dot-Molecule Complexes. *Chem. Rev.* **2016**, *116*, 12865–12919.
- (69) Kerzig, C.; Guo, X.; Wenger, O. S. Unexpected Hydrated Electron Source for Preparative Visible-Light Driven Photoredox Catalysis. *J. Am. Chem. Soc.* **2019**, *141*, 2122–2127.
- (70) Cohn, A. W.; Rinehart, J. D.; Schimpf, A. M.; Weaver, A. L.; Gamelin, D. R. Size Dependence of Negative Trion Auger Recombination in Photodoped CdSe Nanocrystals. *Nano Lett.* **2014**, *14*, 353–358.
- (71) Park, Y.-S.; Bae, W. K.; Pietryga, J. M.; Klimov, V. I. Auger Recombination of Biexcitons and Negative and Positive Trions in Individual Quantum Dots. *ACS Nano* **2014**, *8*, 7288–7296.
- (72) Hou, X.; Kang, J.; Qin, H.; Chen, X.; Ma, J.; Zhou, J.; Chen, L.; Wang, L.; Wang, L.-W.; Peng, X. Engineering Auger recombination in colloidal quantum dots via dielectric screening. *Nat. Commun.* **2019**, *10*, 1750.
- (73) Dong, Y.; Choi, J.; Jeong, H.-K.; Son, D. H. Hot Electrons Generated from Doped Quantum Dots via Upconversion of Excitons to Hot Charge Carriers for Enhanced Photocatalysis. *J. Am. Chem. Soc.* **2015**, *137*, 5549–5554.
- (74) Different terminology exists for describing QDs which become negatively charged by the presence of a surplus electron in the conduction band 1Se state. Here we use “photodoped” and “anionic” to describe these QDs when prepared via irradiation in the presence of reductant.
- (75) Kobayashi, Y.; Nishimura, T.; Yamaguchi, H.; Tamai, N. Effect of Surface Defects on Auger Recombination in Colloidal CdS Quantum Dots. *J. Phys. Chem. Lett.* **2011**, *2*, 1051–1055.
- (76) Wu, K.; Lim, J.; Klimov, V. I. Superposition Principle in Auger Recombination of Charged and Neutral Multicarrier States in Semiconductor Quantum Dots. *ACS Nano* **2017**, *11*, 8437–8447.

- (77) Guyot-Sionnest, P.; Wehrenberg, B.; Yu, D. Intraband relaxation in CdSe nanocrystals and the strong influence of the surface ligands. *J. Chem. Phys.* **2005**, *123*, 074709.
- (78) Singhal, P.; Ghosh, H. N. Hot Charge Carriers in Quantum Dots: Generation, Relaxation, Extraction, and Applications. *ChemNanoMat* **2019**, *5*, 985–999.
- (79) Parobek, D.; Meeder, J. R.; Puthenpurayil, J.; Nippe, M.; Son, D. H. Breaking the short-range proximity requirement in quantum dot/molecular catalyst hybrids for CO<sub>2</sub> reduction via long-range hot electron sensitization. *J. Mater. Chem. A* **2020**, *8*, 12984–12989.
- (80) Orrison, C.; Meeder, J. R.; Zhang, B.; Puthenpurayil, J.; Hall, M. B.; Nippe, M.; Son, D. H. Efficient Redox-Neutral Photocatalytic Formate to Carbon Monoxide Conversion Enabled by Long-Range Hot Electron Transfer from Mn-Doped Quantum Dots. *J. Am. Chem. Soc.* **2021**, *143*, 10292–10300.
- (81) Different batches of CdS QDs yielded sizes ranging between 5.8 and 6.0 nm, however these performed equally well for the described chemistry as long as the molar loading of QDs was kept constant.
- (82) Haram, S. K.; Quinn, B. M.; Bard, A. J. Electrochemistry of CdS Nanoparticles: A Correlation between Optical and Electrochemical Band Gaps. *J. Am. Chem. Soc.* **2001**, *123*, 8860–8861.
- (83) Ingole, P. P.; Markad, G. B.; Saraf, D.; Tatikondewar, L.; Nene, O.; Kshirsagar, A.; Haram, S. K. Band Gap Bowing at Nanoscale: Investigation of CdS<sub>x</sub>Se<sub>1-x</sub> Alloy Quantum Dots through Cyclic Voltammetry and Density Functional Theory. *J. Phys. Chem. C* **2013**, *117*, 7376–7383.
- (84) Martindale, B. C. M.; Hutton, G. A. M.; Caputo, C. A.; Reisner, E. Solar Hydrogen Production Using Carbon Quantum Dots and a Molecular Nickel Catalyst. *J. Am. Chem. Soc.* **2015**, *137*, 6018–6025.
- (85) Gong, K.; Martin, J. E.; Shea-Rohwer, L. E.; Lu, P.; Kelley, D. F. Radiative Lifetimes of Zincblende CdSe/CdS Quantum Dots. *J. Phys. Chem. C* **2015**, *119*, 2231–2238.
- (86) Gong, K.; Zeng, Y.; Kelley, D. F. Extinction Coefficients, Oscillator Strengths, and Radiative Lifetimes of CdSe, CdTe, and CdTe/CdSe Nanocrystals. *J. Phys. Chem. C* **2013**, *117*, 20268–20279.
- (87) Holzer, W.; Penzkofer, A.; Tsuboi, T. Absorption and emission spectroscopic characterization of Ir(ppy)<sub>3</sub>. *Chem. Phys.* **2005**, *308*, 93–102.
- (88) Gisbertz, S.; Pieber, B. Heterogeneous Photocatalysis in Organic Synthesis. *ChemPhotoChem* **2020**, *4*, 456–475.
- (89) Lin, Y.; Guo, J.; San Martin, J.; Han, C.; Martinez, R.; Yan, Y. Photoredox Organic Synthesis Employing Heterogeneous Photocatalysts with Emphasis on Halide Perovskite. *Chem. – Eur. J.* **2020**, *26*, 13118–13136.
- (90) Wang, Y.; Wei, Y.; Song, W.; Chen, C.; Zhao, J. Photocatalytic Hydrodehalogenation for the Removal of Halogenated Aromatic Contaminants. *ChemCatChem* **2019**, *11*, 258–268.
- (91) Vaxenburg, R.; Rodina, A.; Shabaev, A.; Lifshitz, E.; Efros, A. L. Nonradiative Auger Recombination in Semiconductor Nanocrystals. *Nano Lett.* **2015**, *15*, 2092–2098.
- (92) Kharchenko, V. A.; Rosen, M. Auger relaxation processes in semiconductor nanocrystals and quantum wells. *Spectrosc. Isol. Assem. Semicond. Nanocrystals* **1996**, *70*, 158–169.

- (93) MacKenzie, I. A.; Wang, L.; Onuska, N. P. R.; Williams, O. F.; Begam, K.; Moran, A. M.; Dunietz, B. D.; Nicewicz, D. A. Discovery and characterization of an acridine radical photoreductant. *Nature* **2020**, *580*, 76–80.
- (94) Many other deeply reducing conPET catalysts have been described employing other wavelengths of light, however we elected to directly compare catalysts which function with similar wavelengths of light to the QDs (455 nm). For example, acridinium photocatalysts have been employed for two-photon photoreductions of electron-rich aryl chlorides using 390 nm light, but provided no product under our conditions. Based on this report, we calculate a turnover number of 8.2 for the dechlorination of 4-chloroanisole. See: (a) MacKenzie, I. A.; Wang, L.; Onuska, N. P. R.; Williams, O. F.; Begam, K.; Moran, A. M.; Dunietz, B. D.; Nicewicz, D. A. Discovery and Characterization of an Acridine Radical Photoreductant. *Nature* **2020**, *580*, 76–80.
- (95) Owen, J. The coordination chemistry of nanocrystal surfaces. *Science* **2015**, *347*, 615.
- (96) Anderson, N. C.; Chen, Peter. E.; Buckley, A. K.; De Roo, J.; Owen, J. S. Stereoelectronic Effects on the Binding of Neutral Lewis Bases to CdSe Nanocrystals. *J. Am. Chem. Soc.* **2018**, *140*, 7199–7205.
- (97) De Roo, J.; De Keukeleere, K.; Hens, Z.; Van Driessche, I. From ligands to binding motifs and beyond; the enhanced versatility of nanocrystal surfaces. *Dalton Trans.* **2016**, *45*, 13277–13283.
- (98) Morris-Cohen, A. J.; Malicki, M.; Peterson, M. D.; Slavin, J. W. J.; Weiss, E. A. Chemical, Structural, and Quantitative Analysis of the Ligand Shells of Colloidal Quantum Dots. *Chem. Mater.* **2013**, *25*, 1155–1165.
- (99) Anderson, N. C.; Hendricks, M. P.; Choi, J. J.; Owen, J. S. Ligand Exchange and the Stoichiometry of Metal Chalcogenide Nanocrystals: Spectroscopic Observation of Facile Metal-Carboxylate Displacement and Binding. *J. Am. Chem. Soc.* **2013**, *135*, 18536–18548.
- (100) Chen, P. E.; Anderson, N. C.; Norman, Z. M.; Owen, J. S. Tight Binding of Carboxylate, Phosphonate, and Carbamate Anions to Stoichiometric CdSe Nanocrystals. *J. Am. Chem. Soc.* **2017**, *139*, 3227–3236.
- (101) Weinberg, D. J.; He, C.; Weiss, E. A. Control of the Redox Activity of Quantum Dots through Introduction of Fluoroalkanethiolates into Their Ligand Shells. *J. Am. Chem. Soc.* **2016**, *138*, 2319–2326.
- (102) Nepomnyashchii, A. B.; Harris, R. D.; Weiss, E. A. Composition and Permeability of Oleate Adlayers of CdS Quantum Dots upon Dilution to Photoluminescence-Relevant Concentrations. *Anal. Chem.* **2016**, *88*, 3310–3316.
- (103) Hartley, C. L.; Dempsey, J. L. Electron-Promoted X-Type Ligand Displacement at CdSe Quantum Dot Surfaces. *Nano Lett.* **2019**, *19*, 1151–1157.
- (104) Peterson, M. D.; Jensen, S. C.; Weinberg, D. J.; Weiss, E. A. Mechanisms for Adsorption of Methyl Viologen on CdS Quantum Dots. *ACS Nano* **2014**, *8*, 2826–2837.
- (105) Weiss, E. A. Designing the Surfaces of Semiconductor Quantum Dots for Colloidal Photocatalysis. *ACS Energy Lett.* **2017**, *2*, 1005–1013.
- (106) Constantin, T.; Zanini, M.; Regni, A.; Sheikh, N. S.; Juliá, F.; Leonori, D. Aminoalkyl radicals as halogen-atom transfer agents for activation of alkyl and aryl halides. *Science* **2020**, *367*, 1021.

- (107) Constantin, T.; Juliá, F.; Sheikh, N. S.; Leonori, D. A case of chain propagation:  $\alpha$ -aminoalkyl radicals as initiators for aryl radical chemistry. *Chem. Sci.* **2020**, *11*, 12822–12828.
- (108) Hendy, C. M.; Smith, G. C.; Xu, Z.; Lian, T.; Jui, N. T. Radical Chain Reduction via Carbon Dioxide Radical Anion ( $\text{CO}_2^{\bullet-}$ ). *J. Am. Chem. Soc.* **2021**, *143*, 8987–8992.
- (109) Koppenol, W. H.; Rush, J. D. Reduction potential of the carbon dioxide/carbon dioxide radical anion: a comparison with other C1 radicals. *J. Phys. Chem.* **1987**, *91*, 4429–4430.
- (110) Takeda, N.; Poliakov, P. V.; Cook, A. R.; Miller, J. R. Faster Dissociation: Measured Rates and Computed Effects on Barriers in Aryl Halide Radical Anions. *J. Am. Chem. Soc.* **2004**, *126*, 4301–4309.
- (111) Enemærke, R. J.; Christensen, T. B.; Jensen, H.; Daasbjerg, K. Application of a new kinetic method in the investigation of cleavage reactions of haloaromatic radical anions. *J. Chem. Soc. Perkin Trans. 2* **2001**, No. 9, 1620–1630.
- (112) Costentin, C.; Robert, M.; Savéant, J.-M. Fragmentation of Aryl Halide  $\pi$  Anion Radicals. Bending of the Cleaving Bond and Activation vs Driving Force Relationships. *J. Am. Chem. Soc.* **2004**, *126*, 16051–16057.
- (113) Rinehart, J. D.; Schimpf, A. M.; Weaver, A. L.; Cohn, A. W.; Gamelin, D. R. Photochemical Electronic Doping of Colloidal CdSe Nanocrystals. *J. Am. Chem. Soc.* **2013**, *135*, 18782–18785.
- (114) Schimpf, A. M.; Knowles, K. E.; Carroll, G. M.; Gamelin, D. R. Electronic Doping and Redox-Potential Tuning in Colloidal Semiconductor Nanocrystals. *Acc. Chem. Res.* **2015**, *48*, 1929–1937.
- (115) Shulenberger, K. E.; Keller, H. R.; Pellows, L. M.; Brown, N. L.; Dukovic, G. Photocharging of Colloidal CdS Nanocrystals. *J. Phys. Chem. C* **2021**, *125*, 22650–22659.
- (116) Shim, M.; Guyot-Sionnest, P. N-type colloidal semiconductor nanocrystals. *Nature* **2000**, *407*, 981–983.
- (117) Hu, Z.; Shu, Y.; Qin, H.; Hu, X.; Peng, X. Water Effects on Colloidal Semiconductor Nanocrystals: Correlation of Photophysics and Photochemistry. *J. Am. Chem. Soc.* **2021**, *143*, 18721–18732.
- (118) Shim, M.; Wang, C.; Guyot-Sionnest, P. Charge-Tunable Optical Properties in Colloidal Semiconductor Nanocrystals. *J. Phys. Chem. B* **2001**, *105*, 2369–2373.
- (119) Garoz-Ruiz, J.; Perales-Rondon, J. V.; Heras, A.; Colina, A. Spectroelectrochemistry of Quantum Dots. *Isr. J. Chem.* **2019**, *59*, 679–694.
- (120) Honarfar, A.; Mourad, H.; Lin, W.; Polukeev, A.; Rahaman, A.; Abdellah, M.; Chábera, P.; Pankratova, G.; Gorton, L.; Zheng, K.; Pullerits, T. Photoexcitation Dynamics in Electrochemically Charged CdSe Quantum Dots: From Hot Carrier Cooling to Auger Recombination of Negative Trions. *ACS Appl. Energy Mater.* **2020**, *3*, 12525–12531.
- (121) Shiragami, T.; Ankyu, H.; Fukami, S.; Pac, C.; Yanagida, S.; Mori, H.; Fujita, H. Semiconductor photocatalysis: visible light induced photoreduction of aromatic ketones and electron-deficient alkenes catalysed by quantised cadmium sulfide. *J. Chem. Soc. Faraday Trans.* **1992**, *88*, 1055–1061.
- (122) Rajh, T.; Micic, O. I.; Lawless, D.; Serpone, N. Semiconductor photophysics. 7. Photoluminescence and picosecond charge carrier dynamics in cadmium sulfide quantum dots confined in a silicate glass. *J. Phys. Chem.* **1992**, *96*, 4633–4641.

- (123) Wang Congjun; Shim Moonsub; Guyot-Sionnest Philippe. Electrochromic Nanocrystal Quantum Dots. *Science* **2001**, *291*, 2390–2392.
- (124) Tsui, E. Y.; Carroll, G. M.; Miller, B.; Marchioro, A.; Gamelin, D. R. Extremely Slow Spontaneous Electron Trapping in Photodoped n-Type CdSe Nanocrystals. *Chem. Mater.* **2017**, *29*, 3754–3762.
- (125) Bryant, G. W.; Jaskolski, W. Surface Effects on Capped and Uncapped Nanocrystals. *J. Phys. Chem. B* **2005**, *109*, 19650–19656.
- (126) Empedocles S. A.; Bawendi M. G. Quantum-Confined Stark Effect in Single CdSe Nanocrystallite Quantum Dots. *Science* **1997**, *278*, 2114–2117.
- (127) Empedocles, S. A.; Bawendi, M. G. Influence of Spectral Diffusion on the Line Shapes of Single CdSe Nanocrystallite Quantum Dots. *J. Phys. Chem. B* **1999**, *103*, 1826–1830.
- (128) Wang, J.; Ding, T.; Wu, K. Charge Transfer from n-Doped Nanocrystals: Mimicking Intermediate Events in Multielectron Photocatalysis. *J. Am. Chem. Soc.* **2018**, *140*, 7791–7794.
- (129) Houtepen, A. J.; Hens, Z.; Owen, J. S.; Infante, I. On the Origin of Surface Traps in Colloidal II–VI Semiconductor Nanocrystals. *Chem. Mater.* **2017**, *29*, 752–761.
- (130) du Fossé, I.; Lal, S.; Hossaini, A. N.; Infante, I.; Houtepen, A. J. Effect of Ligands and Solvents on the Stability of Electron Charged CdSe Colloidal Quantum Dots. *J. Phys. Chem. C* **2021**, *125*, 23968–23975.
- (131) Langan, J. R.; Liu, K. J.; Salmon, G. A.; Edwards, P. P.; Ellaboudy, A.; Holton, D. M. The Radiation Chemistry of Organic Amides I. A Pulse Radiolysis Study of Solvated Electrons and Alkalimetal-Electron Species in Cyclic Amides. *Proc. R. Soc. Lond. Ser. Math. Phys. Sci.* **1989**, *421*, 169–178.
- (132) Shkrob, I. A.; Marin, T. W. Electron Localization and Radiation Chemistry of Amides. *J. Phys. Chem. A* **2012**, *116*, 1746–1757.
- (133) Huang, H.-M.; McDouall, J. J. W.; Procter, D. J. Radical Anions from Urea-type Carbonyls: Radical Cyclizations and Cyclization Cascades. *Angew. Chem. Int. Ed.* **2018**, *57*, 4995–4999.
- (134) Volz, N.; Clayden, J. The Urea Renaissance. *Angew. Chem. Int. Ed.* **2011**, *50*, 12148–12155.
- (135) Owing to difficulties in measurement of reduction potentials outside the electrochemical windows of ordinary solvents and electrolytes, there are no reports of solution-phase reduction potentials of tetraalkylureas or trialkyl amides, however gas-phase electron affinities suggest that tetraalkyl ureas should be more difficult to reduce than trialkyl amides to the corresponding radical anions. (a) Lecomte, F.; Lucas, B.; Grégoire, G.; Schermann, J. P.; Desfrancois, C. Urea and Methylurea Dipole-Bound Anions. *Phys. Chem. Chem. Phys.* **2003**, *5*, 3120–3125. (b) Lecomte, F.; Lucas, B.; Grégoire, G.; Schermann, J. P.; Desfrancois, C. Structures of Amide-Water Neutral Complexes from Dipole-Bound Anion Formation. *Eur. Phys. J. D.* **2002**, *20*, 449–457.
- (136) Kimura, M.; Miyahara, H.; Moritani, N.; Sawaki, Y. Electroreductive dehalogenation of chlorinated aromatic ethers. Unexpected electrogenerated base-catalyzed reactions. *J. Org. Chem.* **1990**, *55*, 3897–3902.
- (137) Murphy, J. A.; Zhou, S.; Thomson, D. W.; Schoenebeck, F.; Mahesh, M.; Park, S. R.; Tuttle, T.; Berlouis, L. E. A. The Generation of Aryl Anions by Double Electron Transfer to Aryl Iodides from a Neutral Ground-State Organic Super-Electron Donor. *Angew. Chem. Int. Ed.* **2007**, *46*, 5178–5183.



- (138) Yin, H.; Wada, Y.; Kitamura, T.; Sakata, T.; Mori, H.; Yanagida, S. Enhanced Photocatalytic Dechlorination of 1,2,3,4-Tetrachlorobenzene Using Nanosized CdS/TiO<sub>2</sub> Hybrid Photocatalyst under Visible Light Irradiation. *Chem. Lett.* **2001**, *30*, 334–335.
- (139) Alonso, D. A.; Andersson, P. G. Deprotection of Sulfonyl Aziridines. *J. Org. Chem.* **1998**, *63*, 9455–9461.
- (140) Ankner, T.; Hilmersson, G. Instantaneous Deprotection of Tosylamides and Esters with SmI<sub>2</sub>/Amine/Water. *Org. Lett.* **2009**, *11*, 503–506.
- (141) Alonso, E.; Ramón, D. J.; Yus, M. Reductive deprotection of allyl, benzyl and sulfonyl substituted alcohols, amines and amides using a naphthalene-catalysed lithiation. *Tetrahedron* **1997**, *53*, 14355–14368.
- (142) Hyeong Lee, G.; Bok Choi, E.; Lee, E.; Siek Pak, C. An efficient desulfonylation method mediated by magnesium in ethanol. *Int. J. Rapid Publ. Prelim.* **1993**, *34*, 4541–4542.
- (143) Javorskis, T.; Orentas, E. Chemoselective Deprotection of Sulfonamides Under Acidic Conditions: Scope, Sulfonyl Group Migration, and Synthetic Applications. *J. Org. Chem.* **2017**, *82*, 13423–13439.
- (144) Montenegro, M. I. The electrochemical cleavage of protecting groups. *Electrochimica Acta* **1986**, *31*, 607–620.
- (145) Shi, L.; Xia, W. J.; Zhang, F. M.; Tu, Y. Q. A Novel, Efficient, and Highly Selective O-Bn Bond Cleavage Reaction via a Rare K-Induced Electron Transfer Process. *Synlett* **2002**, *2002*, 1505–1507.
- (146) Weissman, S. A.; Zewge, D. Recent advances in ether dealkylation. *Tetrahedron* **2005**, *61*, 7833–7863.
- (147) Protection for the Hydroxyl Group, Including 1,2- and 1,3-Diols. In *Greene's Protective Groups in Organic Synthesis*; John Wiley & Sons, Ltd, 2006; pp 16–366.
- (148) Liu, H.-J.; Yip, J.; Shia, K.-S. Reductive cleavage of benzyl ethers with lithium naphthalenide. A convenient method for debenzylation. *Tetrahedron Lett.* **1997**, *38*, 2253–2256.
- (149) Doni, E.; O'Sullivan, S.; Murphy, J. A. Metal-Free Reductive Cleavage of Benzylic Esters and Ethers: Fragmentations Result from Single and Double Electron Transfers. *Angew. Chem. Int. Ed.* **2013**, *52*, 2239–2242.
- (150) Miyazaki, T.; Maekawa, H.; Yonemura, K.; Yamamoto, Y.; Yamanaka, Y.; Nishiguchi, I. Mg-promoted facile and selective intramolecular cyclization of aromatic  $\delta$ -ketoesters. *Tetrahedron* **2011**, *67*, 1598–1602.
- (151) While reports of the reduction potentials of trialkyl amides are unavailable, comparison of N,N-dimethylbenzamide (E<sub>red</sub> = -2.53 vs. SCE) with methyl benzoate (-2.29 V vs. SCE) illustrates that amides are generally harder to reduce to the radical anion than the analogous esters.
- (152) Amador, A. G.; Sherbrook, E. M.; Yoon, T. P. Enantioselective Photocatalytic [3 + 2] Cycloadditions of Aryl Cyclopropyl Ketones. *J Am Chem Soc* **2016**, *138*, 4722–4725.
- (153) Lu, Z.; Shen, M.; Yoon, T. P. [3+2] Cycloadditions of Aryl Cyclopropyl Ketones by Visible Light Photocatalysis. *J. Am. Chem. Soc.* **2011**, *133*, 1162–1164.
- (154) Huang, X.; Lin, J.; Shen, T.; Harms, K.; Marchini, M.; Ceroni, P.; Meggers, E. Asymmetric [3+2] Photocycloadditions of Cyclopropanes with Alkenes or Alkynes through Visible-Light Excitation of Catalyst-Bound Substrates. *Angew. Chem. Int. Ed.* **2018**, *57*, 5454–5458.

- (155) Tanko, J. M.; Li, X.; Chahma, M.; Jackson, W. F.; Spencer, J. N. Cyclopropyl Conjugation and Ketyl Anions: When Do Things Begin to Fall Apart? *J. Am. Chem. Soc.* **2007**, *129*, 4181–4192.
- (156) Szostak, M.; Spain, M.; Eberhart, A. J.; Procter, D. J. Mechanism of SmI<sub>2</sub>/Amine/H<sub>2</sub>O-Promoted Chemoselective Reductions of Carboxylic Acid Derivatives (Esters, Acids, and Amides) to Alcohols. *J. Org. Chem.* **2014**, *79*, 11988–12003.
- (157) Ichiyanagi, T.; Kuniyama, S.; Shimizu, M.; Fujisawa, T. Regioselective Ring-opening of Cyclopropyl Ketones with Organometallic Reagents. *Chem Lett* **1997**, 1149–1150.
- (158) Agasti, S.; Beattie, N. A.; McDouall, J. J. W.; Procter, D. J. SmI<sub>2</sub>-Catalyzed Intermolecular Coupling of Cyclopropyl Ketones and Alkynes: A Link between Ketone Conformation and Reactivity. *J. Am. Chem. Soc.* **2021**, *143*, 3655–3661.
- (159) Hao, W.; Harenberg, J. H.; Wu, X.; MacMillan, S. N.; Lin, S. Diastereo- and Enantioselective Formal [3 + 2] Cycloaddition of Cyclopropyl Ketones and Alkenes via Ti-Catalyzed Radical Redox Relay. *J. Am. Chem. Soc.* **2018**, *140*, 3514–3517.
- (160) Liu, L.; Montgomery, J. Dimerization of Cyclopropyl Ketones and Crossed Reactions of Cyclopropyl Ketones with Enones as an Entry to Five-Membered Rings. *J. Am. Chem. Soc.* **2006**, *128*, 5348–5349.
- (161) Tamaki, T.; Ohashi, M.; Ogoshi, S. [3+2] Cycloaddition Reaction of Cyclopropyl Ketones with Alkynes Catalyzed by Nickel/Dimethylaluminum Chloride. *Angew. Chem. Int. Ed.* **2011**, *50*, 12067–12070.
- (162) Huang, H.-M.; McDouall, J. J. W.; Procter, D. J. SmI<sub>2</sub>-catalysed cyclization cascades by radical relay. *Nat. Catal.* **2019**, *2*, 211–218.
- (163) Ogoshi, S.; Nagata, M.; Kurosawa, H. Formation of Nickeladihydropyran by Oxidative Addition of Cyclopropyl Ketone. Key Intermediate in Nickel-Catalyzed Cycloaddition. *J. Am. Chem. Soc.* **2006**, *128*, 5350–5351.
- (164) Tamaki, T.; Nagata, M.; Ohashi, M.; Ogoshi, S. Synthesis and Reactivity of Six-Membered Oxa-Nickelacycles: A Ring-Opening Reaction of Cyclopropyl Ketones. *Chem. – Eur. J.* **2009**, *15*, 10083–10091.
- (165) Wang, J.; Wang, L.; Yu, S.; Ding, T.; Xiang, D.; Wu, K. Spin blockade and phonon bottleneck for hot electron relaxation observed in n-doped colloidal quantum dots. *Nat. Commun.* **2021**, *12*, 550.
- (166) Zhu, H.; Song, N.; Lian, T. Charging of Quantum Dots by Sulfide Redox Electrolytes Reduces Electron Injection Efficiency in Quantum Dot Sensitized Solar Cells. *J. Am. Chem. Soc.* **2013**, *135*, 11461–11464.
- (167) Gosztola, D.; Niemczyk, M. P.; Svec, W.; Lukas, A. S.; Wasielewski, M. R. Excited Doublet States of Electrochemically Generated Aromatic Imide and Diimide Radical Anions. *J. Phys. Chem. A* **2000**, *104*, 6545–6551.
- (168) Pandey Anshu; Guyot-Sionnest Philippe. Slow Electron Cooling in Colloidal Quantum Dots. *Science* **2008**, *322*, 929–932.
- (169) Klimov, V. I. Optical Nonlinearities and Ultrafast Carrier Dynamics in Semiconductor Nanocrystals. *J. Phys. Chem. B* **2000**, *104*, 6112–6123.
- (170) Klimov, V. I.; McBranch, D. W. Femtosecond 1P-to-1S Electron Relaxation in Strongly Confined Semiconductor Nanocrystals. *Phys. Rev. Lett.* **1998**, *80*, 4028–4031.
- (171) Cooney, R. R.; Sewall, S. L.; Dias, E. A.; Sagar, D. M.; Anderson, K. E. H.; Kambhampati, P. Unified picture of electron and hole relaxation pathways in semiconductor quantum dots. *Phys. Rev. B* **2007**, *75*, 245311.

- (172) Dana, J.; Maity, P.; Ghosh, H. N. Hot-electron transfer from the semiconductor domain to the metal domain in CdSe@CdS{Au} nano-heterostructures. *Nanoscale* **2017**, 9, 9723–9731.
- (173) Reiss, P.; Carrière, M.; Lincheneau, C.; Vaure, L.; Tamang, S. Synthesis of Semiconductor Nanocrystals, Focusing on Nontoxic and Earth-Abundant Materials. *Chem. Rev.* **2016**, 116, 10731–10819.

Insert Table of Contents Graphic and Synopsis Here.

